

1 **A Unique Vadose Zone Model for Shallow Aquifers: the Hetao**  
2 **Irrigation District, China**

3 Zhongyi Liu<sup>1,2</sup>, Xingwang Wang<sup>1</sup>, Zailin Huo<sup>1\*</sup>, Tammo S. Steenhuis<sup>2\*</sup>

4  
5  
6 <sup>1</sup>Center for Agricultural Water Research in China, China Agricultural University, Beijing, 100083, PR China

7 <sup>2</sup>Department of Biological and Environmental Engineering, Cornell University, Ithaca, NY, USA.

8  
9 Correspondence to: Zailin Huo ([huozl@cau.edu.cn](mailto:huozl@cau.edu.cn))

10 Tammo S. Steenhuis ([tssl@cornell.edu](mailto:tssl@cornell.edu))

35 **Abstract**

36 Rapid population growth is increasing pressure on the world water resources. Agriculture will require crops to be  
37 grown with less water. This is especially the case for the closed Yellow River basin necessitating a better  
38 understanding of the fate of irrigation water in the soil. In this manuscript, we report on a field experiment and  
39 develop a physically based model for the shallow groundwater in the Hetao irrigation district in Inner Mongolia, in  
40 the arid middle reaches of the Yellow River. Unlike other approaches, this model recognizes that field capacity is  
41 reached when the matric potential is equal to the height above the groundwater table and not by a limiting soil  
42 conductivity. The field experiment was carried out in 2016 and 2017. Daily moisture contents at 5 depths in the top  
43 90 cm and groundwater table depths were measured in two fields with a corn crop. The data collected were used for  
44 model calibration and validation. The calibration and validation results show that the model-simulated soil moisture  
45 and groundwater depth fitted well. The model can be used in areas with shallow groundwater to optimize irrigation  
46 water use and minimize tailwater losses.

47 **Key words:** Hydrological model, Shallow aquifer, Equilibrium state, Soil moisture characteristic curve

48 **1 Introduction**

49 With global climate change and increasing human population, much of the world is facing substantial water shortage  
50 (Alcamo et al., 2007). The water crisis has caused widespread concern among public governmental officials and  
51 scientists (Guo and Shen, 2016; Oki and Kanae, 2006). Years of rapid population growth has squeezed the world  
52 water resources. The available fresh water per capita decreased 7500 m<sup>3</sup> from 13400 m<sup>3</sup> in 1962 to 5900 m<sup>3</sup> in 2014  
53 (World Bank Group, 2019).

54 Water supply in China is especially stressed. When averaged over the whole country, available water per capita  
55 is at the water stress threshold of 1700 m<sup>3</sup> per year (Falkenmark, 1989; Brown and Matlock, 2011). It is even less in  
56 the arid to semi-arid Yellow river basin that produces 33% of the total agricultural production in China. To  
57 overcome water shortages in the Yellow river basin, crops are irrigated from surface and groundwater. This  
58 irrigation has directly changed the hydrology of the basin. While, 50 years ago, the semi-arid North China Plain had  
59 springs, shallow groundwater and rivers feeding the Yellow River, at the present rivers and springs have dried up  
60 where groundwater is used for irrigation (Yang et al., 2015a). At the same time, in the arid Inner Mongolia, along  
61 the Yellow River, the once deep groundwater is now within 3 m of the soil surface in the large irrigation projects

62 such as the Hetao irrigation district because of downward percolation of the excess irrigation water that has been  
63 applied.

64 In the Yellow River basin, crop irrigation accounts for 96% of the total water use (Li et al., 2004). Due to the  
65 increased demand for irrigation, the river has stopped flowing downstream for an average of 70 days per year  
66 (Hinrichsen, 2002). Saving water upstream in Inner Mongolia by improved management practices mean that more  
67 water will be available downstream (Gao et al., 2015). In addition, the Hetao district is suffering from salinization  
68 which leads to the land degradation (Guo et al., 2018; Huang et al., 2018) . Salinization is caused by upward  
69 migration of water (and salt) from shallow groundwater table that leads to salt accumulation at the surface (Ren et  
70 al., 2016; Yeh and Famiglietti, 2009). Designing improved management practices to save water and decrease  
71 salinization can be achieved by field trials or with the aid of computer simulation mode measuring the fluxes. Field  
72 trials are time consuming, expensive and only a limited set of water management practices can be investigated.  
73 Models can test many management practices; however, the modeling results are often questionable because they  
74 have not been validated under local field condition and have not been validated for the future conditions. A  
75 combination of field experiments together with models has the benefits of both approaches with few negative effects.

76 Soil moisture content plays a critical role in quantifying the fluxes in the soil (Batalha et al., 2018), especially  
77 in the areas with shallow groundwater area (Gleeson et al., 2016; Jasechko and Taylor, 2015; Venkatesh et al.,  
78 2011a). Drying of the surface soil sets up hydraulic gradient that causes the upward capillary water movement from  
79 the shallow groundwater to sustain the evapotranspiration demands and crop water use (Kahlow et al., 2005; Liu et  
80 al., 2016; Luo and Sophocleous, 2010; Yeh and Famiglietti, 2009).

81 Central to modeling irrigation management practices under shallow groundwater conditions (such as in the  
82 Yellow river basin) is simulating the soil moisture content accurately (Batalha et al., 2018, Gleeson et al., 2016;  
83 Jasechko and Taylor, 2015; Venkatesh et al., 2011a) because the moisture content plays a critical role in the growth  
84 of crops (Rodriguez-Iturbe, 2000), groundwater recharge (Hodnett and Bell, 1986), upward movement of water to  
85 the root zone in areas (Gleeson et al., 2016; Jasechko and Taylor, 2015; Venkatesh et al., 2011a; Batalha et al.,  
86 2018). The latter is unique to shallow groundwater areas where the moisture content and thus the unsaturated  
87 conductivity are high and where the drying of the surface soil sets up hydraulic gradient that causes the upward  
88 capillary movement from the shallow groundwater (Kahlow et al., 2005; Liu et al., 2016; Luo and Sophocleous,

89 2010; Yeh and Famiglietti, 2009). The upward moving water contains salt that is deposit in the root zone and at the  
90 surface.

#### 91 Modeling moisture contents

92 There is tendency with the ever increasing computer power, to include all processes and the highly  
93 heterogeneous field conditions in hydrological models (Asher et al., 2015). In case of simulating moisture contents  
94 these models become complex and often fully distributed in 3-D (Cui et al., 2017). Examples of these fully  
95 developed models are HYDRUS (Šimůnek et al., 1998), SWAP (Dam et al., 1997) and MODFLOW (McDonald and  
96 Harbaugh, 2003; Langevin, et al., 2017). These models have long run times when applied to real world problems. In  
97 addition, calibration effort increases exponentially with the number of model parameters (Rosa et al., 2012; Flint et  
98 al., 2002). This makes the use of the complex models for real time management and decision support cumbersome  
99 where many model runs are needed (Cui et al., 2017).

100 To overcome the disadvantages of the full and completer models, computationally efficient surrogate models  
101 have been developed to speed up the modeling process without sacrificing accuracy or detail. Surrogate models are  
102 known under several names such as metamodels, reduced models, model emulators, proxy models and response  
103 surfaces (e.g., Razavi et al., 2012a; Asher et al., 2015). The complex models we will call “full” or comprehensive  
104 models.

105 Computational efficiency is the main reason for applying surrogate models in place of full models. Other  
106 advantages of surrogate models are shortening the time needed for calibration; identifying insensitive and irrelevant  
107 parameters in the full models (Young and Ratto, 2011). Most importantly, surrogate models allow investigating  
108 structural model uncertainty (Matott and Rabideau, 2008). Finally, surrogate models might be able to deal with  
109 better with the self- organization of complex system prevalent in hydrology than the full models (Hoang et al., 2017.  
110 For example, full models based on small scale physics (Kirchner, 2006) not necessarily can model the repetitive  
111 wetting patterns observed in humid watersheds and for that reason. Simple surrogate models often outperform their  
112 complex counterparts in predicting runoff when a perched water table is present in sloping terrains (Moges et al,  
113 2017; Hoang et al 2017).

114 Surrogate models can be classified in two categories (Todini, 2007; Asher et al., 2015): data driven and  
115 physically derived. Data driven surrogates analyze relationships between the data available and physically derived  
116 surrogates simplify the underlying physics or reduce numerical resolution. In recent years, most emphasis in the

117 research literature has been data driven surrogate approaches (Razavi et al. 2012a). Relatively little research has  
118 been published on physically derived approaches. Despite its popularity, data-driven surrogates can be an inefficient  
119 and unreliable approach to optimizing complex field situations especially when data is scarce such as in  
120 groundwater systems (Razavi et al. 2012b) The physically derived surrogates overcome many of the limitations of  
121 data-driven approaches and are therefore superior over data driven methods (Asher et al., 2015).

122 In the Yellow River basin various models have been developed to simulate the soil water content and water  
123 fluxes. Full models that have been used are the HYDRUS-1D (Ren et al., 2016), and finite difference model  
124 application by Moiwo et al., (2010). Surrogate models for the North China plain where the groundwater is more than  
125 20 m deep have been published by Wang et al. (2001); Kendy et al (2003); Chen et al. (2010); Ma et al. (2013);  
126 Yang et al. (2015, 2017a,b); Li et al., (2017). In these models, the matric potential is ignored, and the hydraulic  
127 potential is equal to the gravity potential and thus the gradient of the hydraulic potential is unity (at least when it is  
128 expressed in head units). Under these conditions the water flux becomes negligible when the soil reaches field  
129 capacity at -33 KPa (equivalent to -3.3 m in head units) at what point the hydraulic conductivity becomes limiting.  
130 These models are not valid for irrigation projects along the Yellow river with shallow groundwater because the  
131 matric potential cannot be ignored over the short distance between the water table and the surface of the soil. Since  
132 the gravity and matric potential are of the same order, the water moves either down to the groundwater or up from  
133 the groundwater to the root zone depending on the matric potential at the soil (Gardner 1958; Gardener et al,  
134 1970a,b). In summary, thus for shallow groundwater at less than 3.3 m from the surface equilibrium is reached (i.e.  
135 fluxes negligible) when hydraulic gradient is zero (i.e., matric potential and gravity potential add up to constant  
136 value) and thus not when the conductivity becomes limited at a matric potential of -33 KPa.

137 For the irrigation perimeters with shallow groundwater in the Yellow River basin, we could find only two  
138 surrogate models developed by Xue et al. (2018) and Gao et al. (2017a, b). These two models do not consider the  
139 dynamics of groundwater depth and matric potential. By including these dynamics more realistic predictions of  
140 moisture contents and upward flow can be obtained and would give better results when extended outside the area  
141 where they are developed for (Wang and Smith, 2004). The reason is that for areas with shallow groundwater,  
142 evapotranspiration sets up hydraulic gradient that causes the upward capillary water movement to sustain the  
143 evapotranspiration demands and crop water use (Kahlowan et al., 2005; Liu et al., 2016; Luo and Sophocleous, 2010;  
144 Yeh and Famiglietti, 2009).

145 Advantages of physically driven surrogates are particularly relevant groundwater studies where water tables are  
146 simulated over entire large area as shown by Brooks et al. (2007). Despite this, Asher et al. (2015) poses that  
147 physically driven methods have not been applied widely to groundwater problems and even fewer with the  
148 interaction of moisture contents in the vadose zone which are key in salinization and plant growth of the many  
149 cropped irrigated field in arid and semi-arid regions. In these water short areas it is extremely important to develop  
150 models that show directions how to save water. The main objective of this study is, therefore, to develop a novel  
151 surrogate model and validating this approach using experimental data collected in a field with shallow groundwater  
152 with the ultimate goal is to save water in irrigation districts. In addition, sensitive and insensitive model parameters  
153 were identified for simulating moisture content in shallow groundwater area to optimize future data collection  
154 efforts. The experimental fields are located in the Hetao irrigation district, Inner Mongolia, China, where on two  
155 maize fields, the moisture content and the groundwater table depth were measured over a two-year period.

156 The surrogate model developed is a one dimensional model simulating the moisture content in the root zone  
157 using the groundwater depth and information of soil moisture characteristic curve. It can be easily adapted to field  
158 scale by including the lateral movement of the regional groundwater. However, over short times, lateral movement  
159 can be neglected in nearly level areas outside a strip of 5-100 m from the river (Saleh et al., 1989) such as deltas and  
160 lakes (Dam et al., 1997; Kendy et al 2003).

## 161 **2 Materials and Methods**

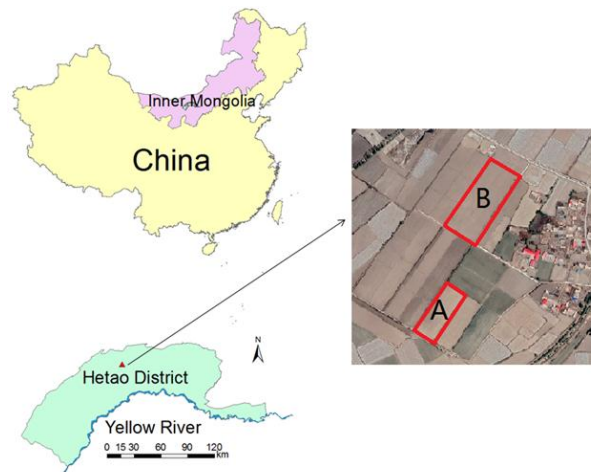
### 162 **2.1 Study Area**

163 The Hetao Irrigation District (HID) is the third largest irrigation district of China. It covers an area of  $1.12 \times 10^6$   
164 ha of which half is irrigated (Xu et al., 2015). About 5 billion  $m^3$  water are diverted from the Yellow River each year  
165 (Xu et al., 2010). The primary irrigation method used is surface flood irrigation (Sun et al., 2013). The groundwater  
166 table is very shallow ranging between 0.5 m to 3 m. The overall hydraulic gradient is 0.1-0.25‰ (Ren et al., 2018).  
167 Soil salinization is serious, and the chemical composition of groundwater salinity mainly consists of NaCl, KCl,  
168  $CaSO_4$ . The Hetao District has a typical arid continental climate with high evaporation and low rainfall. [The average](#)  
169 [annual precipitation](#) is 180 mm and the annual potential evapotranspiration is 2225 mm (Luan et al., 2018). The soil  
170 is mainly alluvial deposits with a silty loam texture. It is frozen 5 to 6 months per year from late November to the  
171 middle of May. Maize and wheat are the main food crops and sunflower is the main cash crop.

172 **2.2 Field experiment and data collection**

173 The experiment was carried out in Fenzidi, Bayannur city (41°9'N, 107°39'E) in the Hetao District in 2016 and  
174 2017 (Fig.1). In 2016, the experiment was carried out separately in site A (about 3100 m<sup>2</sup>) and site B (about 7000 m<sup>2</sup>)  
175 (Fig.1). In 2017, Field B was split into Fields B1 and B2 and experiments were carried out in these two fields. Field  
176 B1 was about 3400 m<sup>2</sup> and B2 about 3600 m<sup>2</sup>. Experimental fields were planted both years with maize. The sowing  
177 dates were April 24, 2016 and May 13, 2017, respectively. The harvest date was October 1<sup>st</sup> in both 2016 and 2017.  
178 The plant growth stages are given in Table 1. The fields were flood irrigated three or four times during the heading  
179 and filling stages starting in late June or early July (Table 2).

180 Precipitation, air temperature, relative humidity, sunshine duration and wind speed were collected from the  
181 weather station at the experimental station. The reference evapotranspiration (ET<sub>0</sub>) was calculated based on the  
182 FAO-Penman-Monteith equation with the daily meteorological data (Allen et al., 1998). Precipitation and ET<sub>0</sub>  
183 during the growing season are shown in Fig. 2. The soil moisture was monitored daily in the top 90 cm using Hydra  
184 Probe Soil Sensors (Stevens Water Monitoring System Inc., Portland, OR, USA) installed in both experimental  
185 fields. Soil moisture was measured at 5 depths: 0-10 cm, 10-30 cm, 30-50 cm, 50-70 cm, and 70-90 cm. The sensors  
186 were connected to data loggers and downloaded via wireless transmission. Calibration was conducted by oven  
187 drying soil samples (Wang et al., 2018; Gao et al., 2017a). The groundwater depth was measured by piezometers  
188 (HOBO Water Level Logger-U20, Onset, Cape Cod, MA, USA) recorded at 30 min intervals.



189  
190 Figure. 1 Location of the field experiment in Hetao irrigation district. The blue line is the Yellow River.

191 Table 1

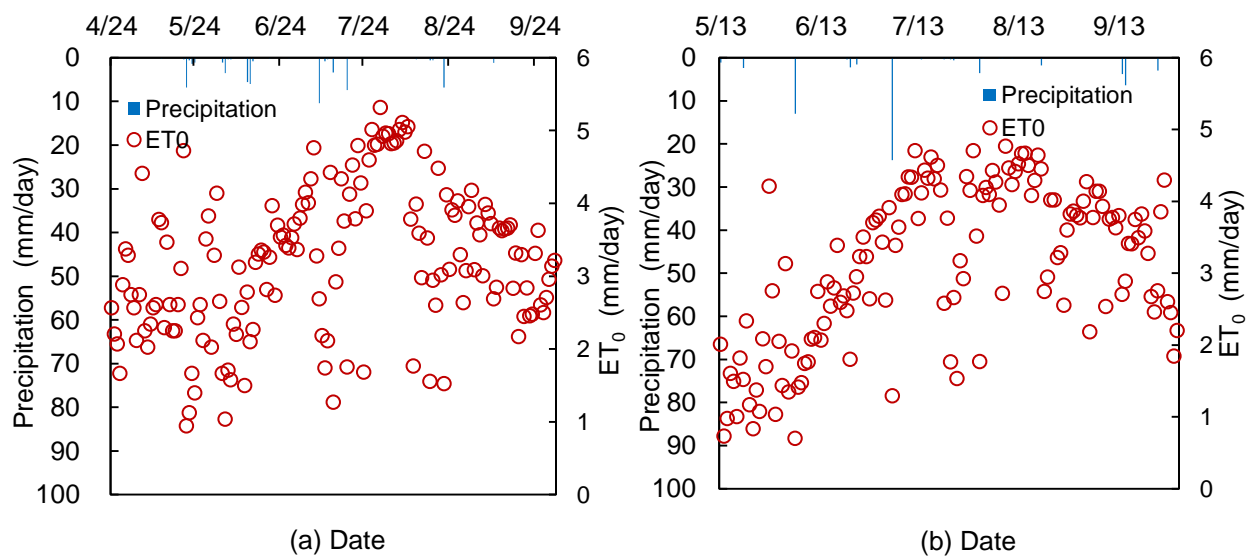
192 *Crop growth stage in 2016 and 2017 for corn growth on the Fenzidi experimental fields in the Hetao district*

Year\Growth stage	seeding	jointing	heading	filling	maturing	harvesting
2016	24-Apr	25-May	16-Jul	6-Aug	3-Sep	1-Oct
2017	13-May	11-Jun	18-Jul	8-Aug	5-Sep	1-Oct

193 Table 2

194 *Irrigation scheduling carried out at Fenzidi experimental fields in 2016 and 2017*

Year	Field	Irrigation events	Date	Irrigation depth(mm)
2016	A	First	July 13	115
		Second	July 26	86
		Third	August 8	122
	B	First	June 23	57
		Second	July 13	119
		Third	July 26	86
Fourth		August 8	122	
2017	B1	First	July 13	153
		Second	July 23	104
		Third	August 9	134
	B2	First	July 13	165
		Second	July 23	107
		Third	August 9	128



195

196 Figure. 2 Daily reference evaporation, ET0, and precipitation during the growing season in (a) 2016 and (b) 2017



197 Soil samples were collected in rings from the same five layers where moisture contents were measured and  
 198 used for determining soil physical properties including soil moisture at field capacity ( $\theta_{fc}$ ), soil moisture at saturation  
 199 ( $\theta_s$ ), dry bulk density ( $\rho$ ), and saturated hydraulic conductivity ( $K_s$ ) (Table 3). For Fields A, B, B1 and B2, the  
 200 saturated hydraulic conductivity was determined by the constant head method. Field capacity was determined at - 33  
 201 kPa and bulk density was determined by oven drying and dividing by the volume of the ring. Soil texture of Fields A  
 202 and B were analyzed with the laser particle size analyzer (Mastersizer 2000, Malvern Instruments Ltd. United  
 203 Kingdom) in the laboratory and are shown in Table 4. The American soil texture classification was used in this  
 204 study. The soils vary from silty loam to silty clay loam.

205 Table 3

206 *Soil physical properties of the Fenzidi experimental fields*

Year	Field	Soil depth (cm)	$\theta_{fc}$ (cm <sup>3</sup> /cm <sup>3</sup> )	$\theta_s$ (cm <sup>3</sup> /cm <sup>3</sup> )	$K_s$ (cm/d)	$\rho$ (g/cm <sup>3</sup> )
2016	A	0-10	0.31	0.47	11.65	1.47
		10-30	0.31	0.47	11.65	1.47
		30-50	0.32	0.51	48.71	1.36
		50-70	0.39	0.44	17.48	1.39
		70-100	0.41	0.44	40.54	1.45
	B	0-10	0.31	0.49	11.39	1.52
		10-30	0.31	0.49	11.39	1.52
		30-50	0.35	0.48	48.68	1.40
		50-70	0.40	0.49	11.06	1.42
		70-100	0.40	0.43	46.68	1.42
2017	B1	0-10	0.36	0.42	5.18	1.52
		10-30	0.36	0.46	5.18	1.52
		30-50	0.35	0.47	11.92	1.38
		50-70	0.42	0.48	4.41	1.37
		70-100	0.21	0.47	6.23	1.69
	B2	0-10	0.37	0.41	4.69	1.44
		10-30	0.37	0.45	4.69	1.44
		30-50	0.39	0.45	6.81	1.42
		50-70	0.42	0.46	10.86	1.42
		70-100	0.29	0.42	10.86	1.76

207 Note:  $\theta_{fc}$  is the soil water content at -33 kPa,  $\theta_s$  is the saturated soil water content,  $K_s$  is the saturated hydraulic  
 208 conductivity,  $\rho$  is the bulk density,  $\psi_h$  is the bubbling pressure.

209 Table 4

210 *Soil texture of Fields A and B*

Site	Depth (cm)	Soil type	Sand (%) (50-2000 $\mu$ m)	Silt (%) (2-50 $\mu$ m)	Clay (%) (0.01-2 $\mu$ m)
A	0-30	silty clay loam	5	75	2
	30-50	silty loam	22	7	8
	50-70	silty clay loam	3	8	17
	70-100	silty loam	39	57	4
B	0-30	silty loam	15	67	18
	30-50	silty loam	35	6	5
	50-70	silty clay loam	3	74	23
	70-100	silty clay loam	8	69	23

211 **2.3 The Shallow Aquifer - Vadose Zone surrogate model**

212 In developing the Shallow Aquifer - Vadose Zone surrogate model for modeling moisture contents in the  
 213 vadose zone, we followed the standards of good modeling practice by Jakeman et al. (2006). We made the model as  
 214 simple as possible, provide justification for our surrogate technique, test the surrogate model performance and  
 215 finally provide detail on the method to encourage discussion on the technique followed.

216 **2.3.1 Theoretical background**

217 For shallow groundwater (less than 3.3 m deep), the matric potential is a function of depth under equilibrium  
 218 conditions. Since the soil moisture characteristic curve for each soil is the relationship of moisture content and  
 219 matric potential, the moisture content is also a function of the depth of the water table under equilibrium conditions.

220 ***Soil moisture characteristic curve***

221 There are several formulations describing the soil moisture characteristic curve (Bauters et al., 2000; Brooks  
 222 and Corey, 1964; Gupta and Larson, 1979; Haverkamp and Parlange, 1986; van Genuchten, 1980); the van  
 223 Genuchten and Brooks & Corey models are widely used in hydrological and soil sciences. Here, we selected the  
 224 Brooks and Corey model for its simplicity.

225 The Brooks-Corey model can be expressed as (Gardner et al., 1970a; Gardner et al., 1970b; Mccuen et al., 1981;  
 226 Williams et al., 1983).

$$S_e = \left(\frac{\varphi_m}{\varphi_b}\right)^{-\lambda} \quad \text{for } |\varphi_m| > |\varphi_b| \quad (1a)$$

$$S_e = 1 \quad \text{for } |\varphi_m| \leq |\varphi_b| \quad (1b)$$

227 in which  $S_e$  is the effective saturation,  $\varphi_b$  is the bubbling pressure (cm),  $\varphi_m$  is matric potential (cm), and  $\lambda$  is the pore  
 228 size distribution index. The effective saturation is defined as

$$S_e = \frac{\theta - \theta_d}{\theta_s - \theta_d} \quad (2)$$

229 in which  $\theta$  is the volumetric moisture content,  $\theta_s$  is the volumetric saturated moisture content,  $\theta_d$  is the residual [air](#)  
 230 [dry moisture](#) content (all in  $\text{cm}^3/\text{cm}^3$ ). Equation 2 can be simplified to the form by setting  $\theta_d = 0$

$$S_e = \frac{\theta}{\theta_s} \quad (3)$$

231 For cases when the groundwater is close to the surface, under equilibrium conditions [when the water flow is](#)  
 232 [negligible, \(i.e., hydraulic potential is constant with depth\)](#), the matric potential can be expressed as height above  
 233 the water table. For our field experiment the bubbling pressure,  $\varphi_b$ , and the pore size distribution index,  $\lambda$ , in the  
 234 Brooks and Corey model can be obtained through a trial and error procedure by using the measured moisture  
 235 content and matric potential derived from the groundwater depth after an irrigation [event when equilibrium state](#)  
 236 was reached [and sum of the gravity potential and matric potential was constant with depth](#).

### 237 2.3.2 Parameters based on soil [moisture characteristic curve](#)

238 The soil of the crop root zone is divided into several soil layers and each soil layer has its specific soil [moisture](#)  
 239 [characteristic curve](#). After a sufficiently large irrigation and rainfall event, the moisture content is at equilibrium  
 240 after the drainage stops. After such an event, the [soil moisture of vadose zone](#) stays at the equilibrium moisture  
 241 content as long as the evapotranspiration is less than upward flux from the groundwater.

#### 242 *Equilibrium moisture content*

243 The equilibrium soil moisture content,  $\theta_{equ}$ , in a layer can be determined by first replacing the matric potential  
 244 in Eq (1a) by the matric potential of the layer  $\varphi_m^{z,h}$  that is dependent [on](#) the depth of the groundwater and depth of  
 245 the soil layer,  $z$ , e.g.

$$\varphi_m^{z,h} = h - z \quad (4)$$

246 where  $\varphi_m^{z,h}$  is the matric potential under equilibrium moisture content at a depth  $z$  below the surface and  $h$  is the  
 247 depth of the groundwater below the surface

$$\theta_{eq}^{z,h} = \theta_s^z \left( \frac{h - z}{\varphi_b^z} \right)^{-\lambda} \quad \text{for } [h - z] > |\varphi_b^z| \quad (5a)$$

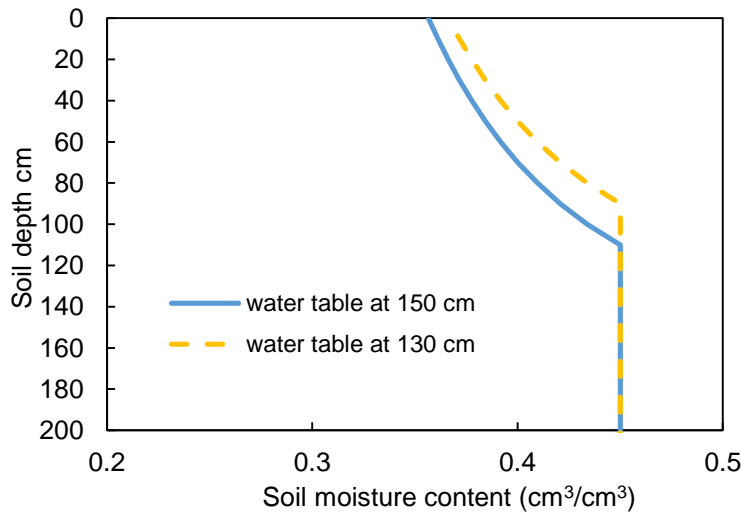
$$\theta_{eq}^{z,h} = \theta_s^z \quad \text{for } [h - z] \leq |\varphi_b^z| \quad (5b)$$

248 where  $\theta_{eq}^{z,h}$  is the equilibrium soil moisture at the depth  $z$  below the surface while the groundwater depth is  $h$ . Note  
 249 that the superscripts  $z$  and  $h$  indicate the dependence on the distance from the soil surface,  $z$ , and the depth,  $h$ , of the  
 250 groundwater table.

### 251 **Drainable porosity**

252 The drainable porosity, or specific yield, is defined as the amount of water drained from the soil for a unit  
 253 decrease of the groundwater table when the soil moisture is at equilibrium. It is a crucial parameter in modeling the  
 254 moisture content in our case or amount of runoff for a shallow perched water table when there is rain (Brooks et al.,  
 255 2007).

256 By subtracting the total moisture content at equilibrium in the profile at the initial water table depth and at the  
 257 new position one unit lower, we obtain the drainable porosity. For example, the area between the orange and blue  
 258 curve is the amount of water drained for a decrease in the water table from 130cm to 150cm (Fig.3).



259 Figure. 3 Illustration of drainable porosity for a soil moisture characteristic curve with a bubbling pressure of 40 cm.

261 The yellow and the blue line are the equilibrium moisture contents for the groundwater depth at 130 and 150 cm,

262 respectively. The area between the two lines represents the amount of water for the decrease of groundwater table  
263 drained from the profile when the groundwater decreases from 130 to 150 cm.

264 The total water content amount of the soil over a prescribed depth with a water table at depth  $h$  can be  
265 expressed as

$$W_{eq}^h = \sum_{j=1}^n L_j \overline{(\theta_{eq}^{z,h})}_j \quad (6)$$

266 where  $\overline{\theta_{eq}^{z,h}}$  is the average equilibrium moisture content of layer  $j$  for  $h$  taken at the midpoint of the layer,  $n$  is the  
267 number of layers in the profile,  $L_j$  is the height of soil layer  $j$ . And the drainable porosity,  $\mu^h$ , with the groundwater  
268 at depth  $h$ , can simply be found as

$$\mu^h = \frac{W_{eq}^{h-\Delta h} - W_{eq}^{h+\Delta h}}{2\Delta h} \quad (7)$$

269 where  $\Delta h = 0.5L_j$ .

### 270 **2.3.3 Calculating fluxes in the soil**

271 The model accounts for the downward flux due to the irrigation and rainfall, evapotranspiration by plants and  
272 soil, and upward flux from the groundwater to satisfy some or all the evapotranspiration demand by the crop and soil.  
273 There are sets of rules implemented in an Excel spreadsheet to calculate the fluxes.

#### 274 *Evapotranspiration*

- 275 1. The plant evapotranspiration was calculated in two steps. First the daily reference evapotranspiration ( $ET_0$ )  
276 was calculated by Penman-Monteith equation (Allen et al., 1998). We assumed that the moisture content  
277 was limiting therefore the plant evapotranspiration rate was obtained by multiplying the reference  
278 evapotranspiration by a crop coefficient. Values for the crop coefficients were calibrated according to the  
279 water balance in the soil and found to agree with published values for stage of crop development and soil  
280 salinity.
- 281 2. (a) On days without rain or irrigation, the evapotranspiration lowers the water table and the moisture  
282 content in the soil decreases due to upward movement of water to the plant roots and soil surface.  
283 (b) On days with rain or irrigation, the potential evapotranspiration is subtracted from the irrigation and/or  
284 rainfall and water moves downward.

#### 285 *Upward flux from groundwater*

286 3. The upward flux from the groundwater,  $U_g^h$ , is either limited by the potential **evapotranspiration** or the  
 287 maximum flux of groundwater. The maximum flux,  $U_{g,max}^h$ , depends on the depth of the groundwater, the  
 288 type of soil **moisture** characteristic curve, and the condition at the surface (Gardner, 1958). These equations  
 289 have an exponential form (Gardner, 1958; Yang et al., 2011; Zammouri, 2001),

$$U_{g,max}^h = \frac{a}{e^{bh} - 1} \quad \text{for } U_g^h \leq ET_p \quad (8)$$

290 where a and b are constants and  $ET_p$  is the potential evapotranspiration. The upward flux from the  
 291 groundwater can be written as:

$$U_g^h = \min(ET_p, U_{g,max}^h) \quad (9)$$

292 On days without rain or irrigation, the soil moisture content is calculated by taking the difference of  
 293 the equilibrium moisture content associated with the change in depth of groundwater. If in addition the  
 294 upward flux is less than evapotranspiration, the difference between the upward **flux** and the  
 295 evapotranspiration is extracted out of the root zone according to a predetermined distribution,  $r_j$ , e.g.,

$$\overline{(\theta^{z,h,t})}_j = \overline{(\theta^{z,h,t-\Delta t})}_j + \overline{(\theta_{eq}^{z,h,t})}_j - \overline{(\theta_{eq}^{z,h,t-\Delta t})}_j - \frac{r_j(K_c ET_p - U_g^h)}{L_j} \quad (10)$$

296 Where  $\overline{(\theta^{z,h,t})}_j$  is the average soil moisture content at time  $t$  of layer  $j$ ,  $\overline{(\theta_{eq}^{z,h,t})}_j$  is the average equilibrium  
 297 soil moisture content of layer  $j$  when the groundwater depth is  $h$  at time  $t$ ,  $K_c$  is a reduction factor of the  
 298 potential evapotranspiration for saline soil water and canopy and  $r_j$  is the root function that determines the  
 299 portion of the evapotranspiration is taken up by the roots in layer  $j$ . The value  $z$  is taken at the midpoint of  
 300 layer  $j$ . The time  $t$  is expressed in days and time,  $t-\Delta t$ , is the previous day.

### 301 ***The downward flux***

302 4. The rules for downward flux on days with the effective rain and/or irrigation are relatively simple. If the net  
 303 flux at the surface (irrigation plus rainfall minus actual **evapotranspiration**) is greater than needed to bring  
 304 the soil up to equilibrium moisture content, the groundwater will be recharged **and the distance to soil**  
 305 **surface decreases** and the moisture content will be equal to the equilibrium moisture content at the new  
 306 depth.

307 5. When the groundwater is not recharged, the following water balance will be calculated: the rainfall and the  
 308 irrigation are added to first layer. This layer will be brought up to the equilibrium moisture content and the

309 remaining water fills up the next layer to the equilibrium moisture content and so on. The calculations can  
 310 be expressed as follows:

$$\overline{(\theta^{z,h,t})}_j = \min \left[ \overline{(\theta_{eq}^{z,h,t})}_j, \overline{(\theta^{z,h,t-\Delta t})}_j + \frac{R_{j-1}\Delta t}{L_j} \right] \quad (11)$$

311 where for  $j \geq 2$ ,  $R_{j-1}$  is the flux from the layer above and equals

$$R_{j+1} = R_j - \frac{\left( \overline{(\theta^{z,h,t})}_j - \overline{(\theta^{z,h,t-\Delta t})}_j \right) L_j}{\Delta t} \quad (12)$$

312 For  $j=1$ ,  $R_j$  is equal to the rainfall plus the irrigation amounts minus potential evaporation

### 313 **Groundwater table depth**

314 6. The groundwater in Hetao irrigation district has a small hydraulic gradient of 0.10-0.25% (Ren et al., 2016).  
 315 In addition, the soil varies from a silt loam to a clay loam (Table 4) that has saturated hydraulic  
 316 conductivity of less than 2 m/day. This means that the lateral fluxes are small compared the vertical fluxes  
 317 and can therefore neglected for the calculation of the groundwater depth. Based on this assumption, the net  
 318 change in groundwater depth,  $\Delta h$ , can be calculated on days without rainfall or irrigation as

$$\Delta h = \frac{U_g^h}{\mu^h} \quad (13a)$$

319 and days with rain or irrigation as

$$\Delta h = -\frac{R_5}{\mu^h} \quad (13b)$$

320 where the upward flux,  $U_g^h$ , is calculated with Eq 9, the percolation of the bottom layer  $R_5$  with Eq 12 and the  
 321 drainable porosity,  $\mu^h$  with Eq 7. When the groundwater is close to the surface, the drainable porosity is zero. This  
 322 would make the change in groundwater infinite. Thus, we limited the maximum decrease in groundwater after the  
 323 irrigation event to be 10-20 cm based on field observations.

### 324 **2.3.4 Model calibration and validation**

325 The soil moisture contents were measured from May 30<sup>th</sup> to September 25<sup>th</sup> in 2016 and 2017. Groundwater  
 326 depth was observed from June 13<sup>th</sup> to September 26<sup>th</sup> in 2016 and 2017. For the convenience of simulation, the  
 327 period of June 13<sup>th</sup> to September 25<sup>th</sup> was set as the simulation period. The model parameters were calibrated with  
 328 the 2016 data and the validation with data collected in 2017 growing seasons. Soil moisture content of the top 90 cm

329 (0-10 cm, 10-30 cm, 30-50 cm, 50-70 cm, 70-90 cm) and the groundwater depth were simulated for model  
 330 calibration and validation.

331 Relatively few parameters can be calibrated in the Shallow Aquifer-Vadose Zone Model. These are the crop  
 332 coefficients  $K_c$  value, the two groundwater parameters and the root function. The other input data needed for model  
 333 were the parameters in the Brooks and Corey equation (e.g.,  $\theta_s, \theta_d, \varphi_b, \lambda$ .) and were obtained by fitting the equation  
 334 to the soil moisture characteristic curve of each layer of the soil. The saturated moisture content was measured  
 335 independently as well and agreed with values obtained from the fit. Reference evapotranspiration was calculated  
 336 directly from observed meteorological data.

337 For better understanding the model fitting performance, statistical indicators were used to evaluate the  
 338 hydrological model goodness-of-fit (Ritter and Muñoz-Carpena, 2013). The statistical indicators including the mean  
 339 relative error (*MRE*) (Dawson et al., 2006), the root mean square error (*RMSE*) (Abrahart and See, 2000; Bowden et  
 340 al., 2002), the Nash-Sutcliffe efficiency coefficient (*NSE*) (Nash and Sutcliffe, 1970), the regression coefficient (*b*)  
 341 (Xu et al., 2015), the determination coefficient ( $R^2$ ) and the regression slope (Krause et al., 2005) were used to  
 342 qualify the model fitting performance during the model calibration and validation in this study. These statistical  
 343 indicators can be expressed as follows:

$$344 \quad MRE = \frac{1}{N} \sum_{i=1}^N \frac{(P_i - O_i)}{O_i} * 100\% \quad (14)$$

$$345 \quad RMSE = \sqrt{\frac{1}{N} \sum_{i=1}^N (P_i - O_i)^2} \quad (15)$$

$$346 \quad NSE = 1 - \frac{\sum_{i=1}^N (P_i - O_i)^2}{\sum_{i=1}^N (O_i - \bar{O})^2} \quad (16)$$

$$347 \quad b = \frac{\sum_{i=1}^N O_i * P_i}{\sum_{i=1}^N O_i^2} \quad (17)$$



348

$$R^2 = \left[ \frac{\sum_i^N (O_i - \bar{O})(P_i - \bar{P})}{\left[ \sum_i^N (O_i - \bar{O}) \right]^{0.5} \left[ \sum_{i=1}^N (P_i - \bar{P}) \right]^{0.5}} \right]^2 \quad (18)$$

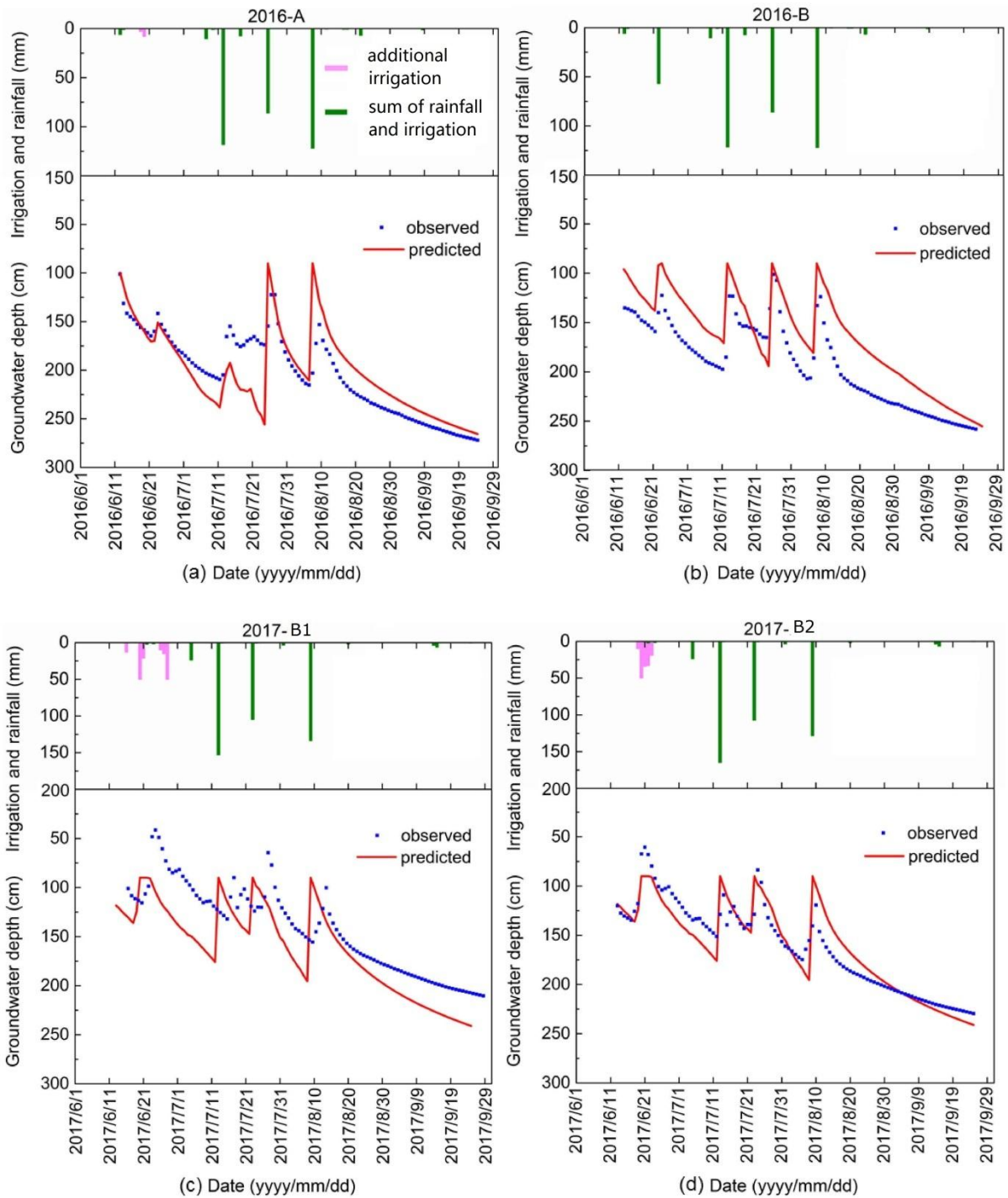
349 where  $N$  is the total number of observations,  $O_i$  and  $P_i$  are the  $i^{\text{th}}$  observed and predicted values ( $i=1, 2, \dots, N$ ), and  
 350  $\bar{O}$  and  $\bar{P}$  are the mean observed values and mean predicted values, respectively. For  $MRE$  and  $RMSE$ , the values  
 351 closest to 0 indicates good model predictions.  $NSE=1.0$  means a perfect fit, and the negative  $NSE$  values indicate  
 352 that the mean observed value is a better predictor than the simulated value (Moriasi et al., 2007). For  $b$  and  $R^2$ , the  
 353 values closest to 1 indicates good model predictions.

### 354 **3 Results**

355 In this section, we present first the 2016 and 2017 experimental observations of the Fenzidi experimental fields  
 356 in the Hetao irrigation district (Fig.1). This is followed by the calibration and validation of the Shallow Aquifer-  
 357 Vadose Zone Model of moisture content in each of the five layers and the groundwater table depth.

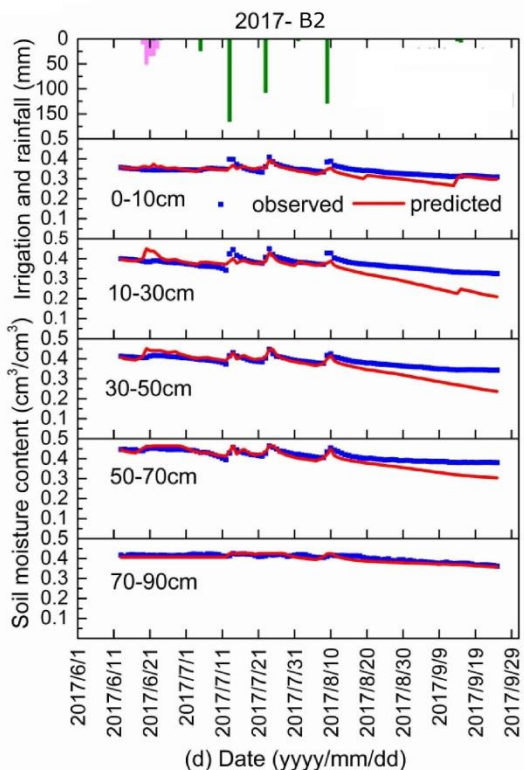
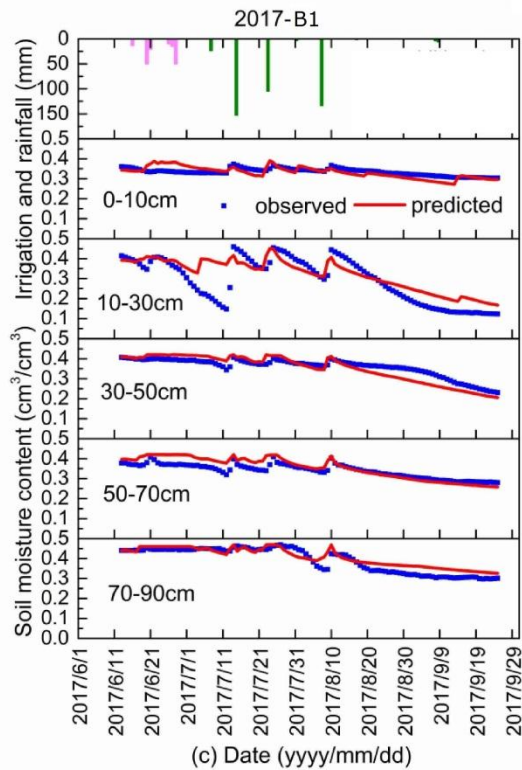
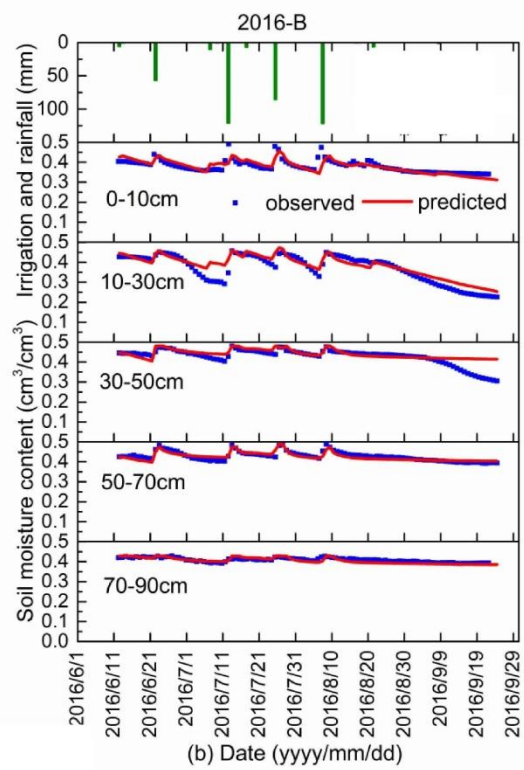
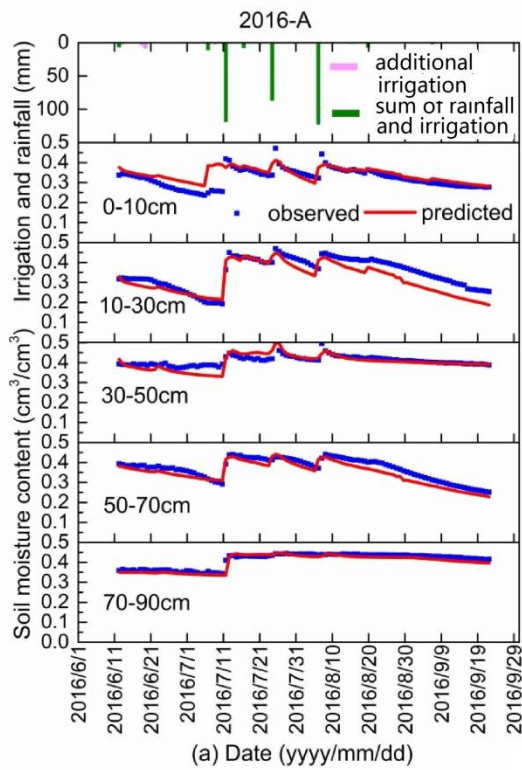
#### 358 **3.1 Results of the field experiment**

359 The total precipitation at the experimental during growing season was 62 mm in 2016 and 67 mm in 2017. The  
 360 maximum daily rainfall was 23 mm in July 2017 (Fig. 2). The reference evapotranspiration varied between 1  
 361 mm/day to 5.5 mm/day and the total  $ET_0$  was 517 mm and 442 mm in the growing seasons during 2016 and 2017,  
 362 respectively (Fig.2). Daily observation consisted of groundwater depth (blue spheres, Fig.4) and soil moisture  
 363 content at five soil depths up to 90 cm (blue spheres, Fig.5) and for Fields A and B in 2016 and Fields B1 and B2 in  
 364 2017.



365  
 366 Figure.4 Simulated and observed groundwater depth during the growing period for the Fenzidi experimental fields  
 367 in the Hetao irrigation district: (a,b) calibration in 2016 and (c,d) validation in 2017. (Notes: Additional irrigation  
 368 means the irrigation recharge from the adjacent field which leads to the water table rise and was not planned).

369



370

371

372 Figure. 5 Simulated and observed soil moisture content for five soil depths during the growing period for the Fenzidi  
373 experimental fields in the Hetao irrigation district: (a, b) calibration in 2016 and (c, d) validation in 2017.

### 374 3.1.1 Groundwater observations

375 In 2016, the groundwater depth was generally more than 100 cm except during the last two irrigation events on  
376 Field B when it reached a depth of 72 cm for one or two days (Fig. 4). In 2017, groundwater tables were slightly  
377 closer to the surface than in 2016, especially in Field B2. The minimum groundwater depth was 61 cm on June 21,  
378 2017 in Field B2 after an irrigation event.

379 In general, groundwater rose during an irrigation event and then decreased slowly due to upward movement of  
380 water to the plant roots to meet the transpiration demand. However, in the beginning of the growing season, we can  
381 see that the water table increased without an irrigation event. This occurred on Field A on June 24, 2016 and Fields  
382 B1 and B2 on June 20, 2017 (Fig. 4). This is curious and could be due to water originating from irrigation in a  
383 nearby field.

384 The water table at the end of the period of observation on September 25, 2016 is approximately 2 m deep,  
385 whereas on June 15, 2017, the depth decreased to around 125 cm. This is due to an irrigation application after the  
386 crops were harvested to leach the salt from the surface to deeper in the profile bringing the water table up to near the  
387 surface. Evapotranspiration during the winter is small but sufficient to bring the water table down. There was also a  
388 rainfall event on June 5, 2017 of 13 mm (Fig. 2) before the water table was measured, increasing the water level.

### 389 3.1.2 Soil Moisture

390 Moisture contents are shown for the five layers and the two fields for 2016 and 2017 in Fig. 5. The moisture  
391 contents were near saturation when irrigation water was added and subsequently decreased (Fig. 5). For example,  
392 the soil moisture content changed in the 0-10 cm layer from  $0.26 \text{ cm}^3/\text{cm}^3$  to  $0.42 \text{ cm}^3/\text{cm}^3$  after the irrigation on  
393 July 13, 2016 in Field A and then gradually decreased to  $0.34 \text{ cm}^3/\text{cm}^3$ . The moisture content decreased faster in the  
394 10-30 cm depth than at any other depth for Fields A, B and B1 but not for Field B2. The moisture content in Field A  
395 also showed a decrease at the 50-70 cm depth. For all plots, the moisture content at the 70-90 cm depth stayed nearly  
396 constant and only decreased during the growing season when the water table decreased below the 150 cm depth (Fig.  
397 5). In Field A, the initial moisture content when the observation started was less than saturation and then after the  
398 first irrigation, remained close to the saturated moisture content.

399 It is interesting that while the soil profile was saturated (Fig. 4), the groundwater table was between 75-100 cm  
400 (Fig. 5). Before equilibrium moisture content was reached the water table was likely near the surface during the  
401 irrigation event. Because the drainable porosity was extremely small, even a minimum amount of evapotranspiration  
402 or drainage would cause the water table to decrease to roughly the height of the capillary fringe equal to the  
403 bubbling pressure,  $\varphi_b$ , in Eq. 5. The values of bubbling pressure are listed in Table 5.

### 404 3.1.3 Soil moisture characteristic curve

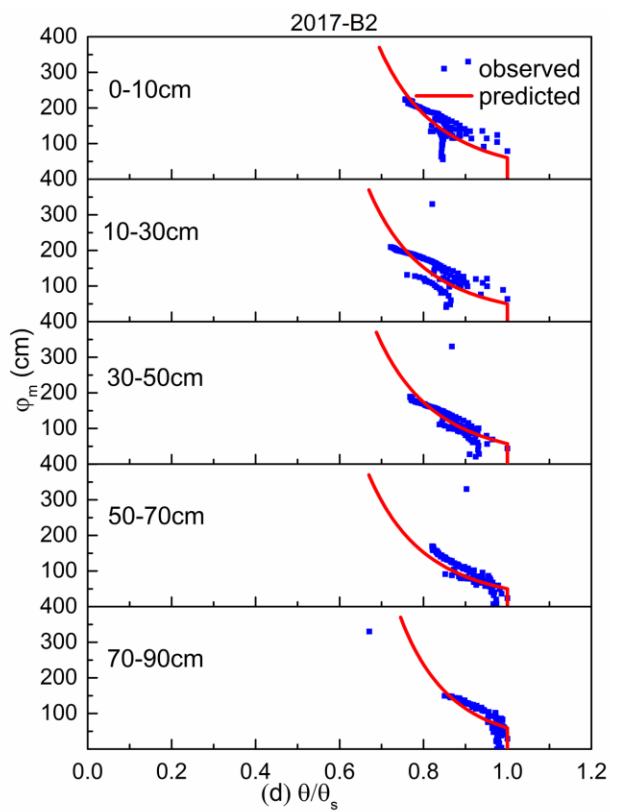
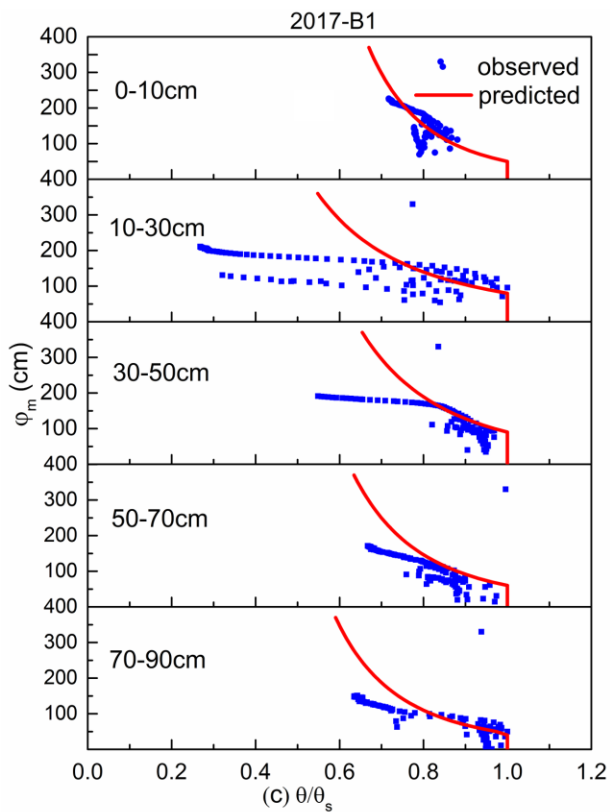
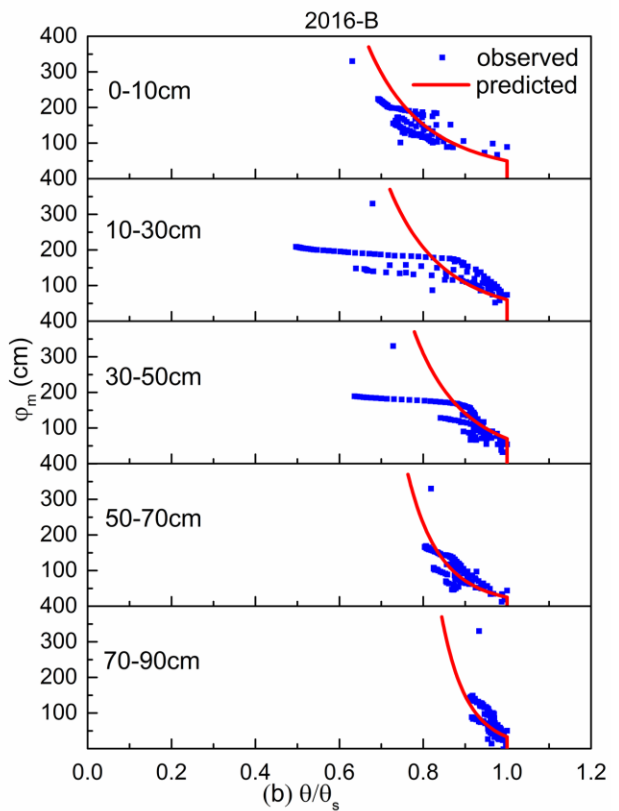
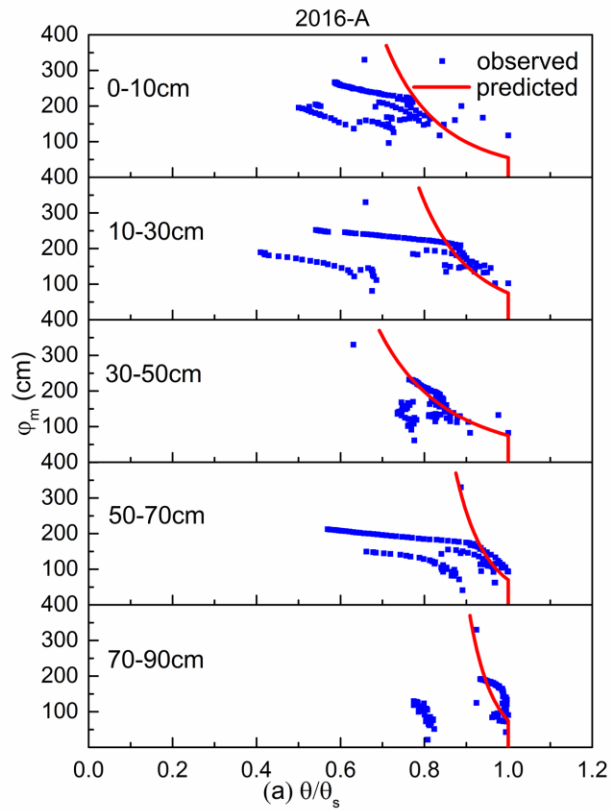
405 In 2016 and 2017, the observed reduced moisture contents were plotted versus the height above the water table  
406 for the five soil layers of the two field sites in Fig. 6. These plots were used to define the soil moisture characteristic  
407 curves which were of critical importance in simulating the moisture contents.

408 To define the soil moisture characteristic curve, the Brooks-Corey equation (Eq. 1) was fitted through the  
409 points closest to saturation at each matric potential representing the equilibrium conditions after an irrigation event.  
410 The fitted parameter values are shown in Table 5. Points to the left of the soil moisture characteristic curve are a  
411 result of evapotranspiration drying out the soil when the upward movement of water was insufficient to replenish the  
412 moisture content in these layers and thus matric potential and groundwater depth were not in equilibrium. In  
413 addition, the few points to the right indicate the soil moisture was greater than the equilibrium moisture content.  
414 Many of the outlier soil moisture contents occurred in the layer from 0-10 cm indicating that the soil was still  
415 draining after a rainfall event shortly before the measurements. Thus, the soil was not at the equilibrium moisture  
416 content.

417 The saturated moisture contents in Table 5 agree in general with the one measured in Table 1 but are not exact.  
418 This is not a surprise as the alluvial soil deposited by the rivers with layers vary over short distances. The variation  
419 within the field was also obvious from the soil's physical measurements. Fields B1 and B2 are within Field B. The  
420 soil's physical properties of the various layers (Table 4) were not the same for the three sites, clearly showing the  
421 variability within the field.

422 Generally, large values of pore size index coefficient  $\lambda$  are for sandy soils and lower values are for clay soils  
423 (Bahmani and Bayram, 2018). We find this to be true for our site: for example, in Field A, the  $\lambda=0.23$  corresponds to  
424 a sandy layer with only 8% clay in the 30-50 cm layer (Tables 4 and 5). In the 70-90 cm layer of Field B, the  $\lambda=0.07$   
425 corresponds with the clay layer of 23% clay. In addition, bubbling pressure,  $\varphi_b$ , are greater for soils with a large

426 clay content (Bahmani and Bayram, 2018). This is demonstrated for Field A in the 10-30 cm layer where the  
427 bubbling pressure of 75 cm corresponded with the clay layer of 20% clay. However, the correspondence between  
428 [Tables 4 and 5](#) is not always perfect. This is especially obvious for the layer of 70-90 cm in Field A where the values  
429 in [Table 5](#) clearly [indicate](#) that the soil has a dense clay layer; however, the soil description in [Table 4](#) shows that the  
430 soil is 39% sand. This is due to the alluvial deposition patterns with changes in soil texture over short distances as  
431 mentioned before.



433 Figure.6 Soil moisture characteristic curve of the four experiment fields for the Fenzidi experimental fields. The red  
 434 line is the fit with the Brooks and Corey equation.

435 Table 5

436 *Fitted Brooks and Corey parameters for the soil moisture characteristic curve*

Soil depth	Lamda( $\lambda$ )				bubbling pressure ( $\varphi_b$ )cm				saturated moisture content (cm <sup>3</sup> /cm <sup>3</sup> )			
	Field	A	B	B1	B2	A	B	B1	B2	A	B	B1
0-10	0.18	0.2	0.2	0.2	55	50	50	60	0.47	0.49	0.42	0.41
10-30	0.15	0.18	0.17	0.2	75	60	70	50	0.47	0.48	0.46	0.45
30-50	0.23	0.15	0.25	0.2	75	70	50	57	0.51	0.48	0.47	0.45
50-70	0.08	0.1	0.25	0.2	70	25	30	50	0.44	0.49	0.48	0.46
70-90	0.06	0.07	0.3	0.16	75	33	45	59	0.44	0.43	0.47	0.42

437 3.2 Modeling results

438 The four parameters that can be calibrated in the Shallow Aquifer-Vadose Zone Model are the crop coefficients  
 439  $K_c$  value and the root function both related to removal of water by the atmosphere and the two groundwater  
 440 parameters that determine the upward movement of water from the groundwater.

441 3.2.1 Calibration of the parameters related to moisture content

442 The first step in the calibration was to fit the  $K_c$  value from the water balance. From the moisture contents and  
 443 the groundwater depth, we can calculate approximately the amount of water lost to evapotranspiration. By  
 444 comparing these values to the reference evapotranspiration calculated with the Penman-Monteith equation, we found  
 445 that initially during the early stages the crop coefficient was 0.3 until the filling stage and then increased to 0.7  
 446 during the filling stage to the maturing stage (Table 6). These values are in accordance with the findings of Katerji et  
 447 al., (2003) that salinity reduces the evapotranspiration (Katerji et al., 2003). According to the observed total salt  
 448 content, the mean total salt content of experiment field in 0-100cm soil layer during crop growth period were  
 449 2.29g/kg in field A, 1.79g/kg in field B, 2.33g/kg in Field B1, 20.9g/kg in Field B2, respectively.

450 The second step was calibrating the moisture content by adapting the root function indicating from what layers  
 451 the water was taken up. Calibration was done manually by trial and error. We found that we could use the same root  
 452 function for Fields A, B, B1, and B2 (Table 6). The calibrated soil moisture contents of the five soil layers for the  
 453 two fields in general are in agreement with the measured values in 2016 (Fig 5a, b) with the coefficient of



454 determination  $R^2$  ranging between 0.48 to 0.94 with slopes of around 1; the mean relative error (MRE) between -9.38%  
 455 and 6.96% and the root mean square error (RMSE) varied from 0.01 to 0.04 cm<sup>3</sup>/cm<sup>3</sup> for the five layers (Table 7-1).  
 456 Finally, the parameters behaved physically realistically as water was extracted from shallow layers when the  
 457 groundwater was close to the surface and from the deeper layers when the groundwater and the associated capillary  
 458 fringe went down.

459 Table 6  
 460 Calibrated parameter values of the Vadose Zone Shallow Aquifer model

Items	Date	Calibrated value
Crop parameter, Kc	June 13-July 14	0.3
	July 15-September 25	0.7
	June 13-August 7	0.2
0-10cm	August 8-September 3	0.1
	September 4-October 1	0.1
	June 13-August 7	0.4
10-30cm	August 8-September 3	0.4
	September 4-October 1	0.4
	June 13-August 7	0.3
Root function, r <sub>j</sub>	30-50cm	0.3
	September 4-October 1	0.3
	June 13-August 7	0.1
50-70cm	August 8-September 3	0.2
	September 4-October 1	0.1
	June 13-August 7	0
70-90cm	August 8-September 3	0
	September 4-October 1	0.1
	a	Field A
b		0.021
a	Field B, B1, B2	110
B		0.025

461 3.2.2. Validation of the parameters related to moisture content

462 The moisture contents predicted by the Shallow Aquifer-Vadose Zone Model were validated with the 2017 data  
 463 on Fields B1 and B2. Although the validation statistics of the five layers were slightly worse than for calibration in

464 Table 7, the overall fit was still good as shown in Fig. 5c, d. The coefficient of determination varied between 0.39  
 465 and 0.90. The MRE varied between -9.34% and 19.48%, and the mean RMSE range was from 0.01 to 0.07 cm<sup>3</sup>/cm<sup>3</sup>  
 466 for the five soil layers (Table 7-2).

### 467 3.2.3 Calibration of the parameters related to groundwater depth

468 The final step was to calibrate the groundwater table coefficients with the 2016 data for both fields. We found  
 469 that for fields not in the same location (e.g., A, B) the subsurface was sufficiently different so that the same set of  
 470 parameters could not be used (Table 6). The difference between the calibrated parameters for the two fields was  
 471 small (Table 6). The measured and simulated groundwater depths were in good agreement with the chosen set of  
 472 parameters (Fig. 4a, b) with coefficient of determination  $R^2$  being 0.67 for Field A and 0.85 for Field B (Table 7-1).  
 473 Only from July 15 to July 25 did the observed water table on Field B decrease slower than the simulated water table.  
 474 This is partly related to the fact that the properties of the soil below 90 cm were not measured, and the assumption  
 475 was made the soil moisture characteristic curve below 90 cm was the same as that from 70-90 cm. Thus the  
 476 drainable porosity of the soil which is very sensitive parameter might be different than what was used in the model.  
 477 Another reason might be that the equation for upward movement might be too simple. Other statistical indicators  
 478 show a good fit as well (Table 7-1).

479 Table 7-1

480 Model statistics for calibration of the Shallow Aquifer model in 2016 Mean relative error, MRE; root mean square  
 481 error, RMSE; Regression slope; Coefficient of determination, R<sup>2</sup>; Regression coefficient, b.

Calibration (2016)								
		SWC (cm <sup>3</sup> /cm <sup>3</sup> )						GWD (cm)
		0-10cm	10-30cm	30-50cm	50-70cm	70-90cm	0-90cm	
A	MRE(%)	6.96	-9.38	-1.72	-5.74	-2.31	-2.44	-16.27
	RMSE(cm <sup>3</sup> /cm <sup>3</sup> or cm)	0.04	0.04	0.02	0.03	0.01	0.03	46.52
	Regression Slope	0.51	0.94	1.34	1.01	1.05	0.50	0.50
	NSE	0.32	0.64	0.11	0.76	0.48	0.74	-0.31
	R <sup>2</sup>	0.49	0.85	0.72	0.92	0.94	0.79	0.67
	b	1.05	0.91	0.99	0.95	0.98	0.97	0.81
B	MRE(%)	-0.69	4.21	3.83	-0.41	-0.87	1.22	1.89
	RMSE(cm <sup>3</sup> /cm <sup>3</sup> or cm)	0.02	0.03	0.03	0.01	0.01	0.02	18.28
	Regression Slope	0.93	0.72	0.37	0.76	1.14	0.76	0.85
	NSE	0.69	0.80	0.34	0.74	-0.19	0.77	0.81
	R <sup>2</sup>	0.73	0.85	0.48	0.74	0.69	0.77	0.85
	b	0.99	1.03	1.03	0.99	0.99	1.00	1.02

482 3.2.4 Validation of the parameters related to groundwater depth

483 Since Fields B1 and B2 are in the same location as Field B, we used the same set of groundwater parameters  
 484 for the three fields (Table 6). The resulting fit between observed and predicted daily groundwater depths for Fields  
 485 B1 and B2 in 2017 was better than for the calibration in 2016 (Fig. 4c, d) with  $R^2$  values of 0.84 for Field B1 and  
 486 0.86 for Field B2 (Table 7-2). In both cases, the slope of the regression line was close to 1. The other statistics  
 487 indicated a good fit as well (Table 7-2) with the mean relative error (MRE) being -0.05 for Field B1 and -0.02 for  
 488 Field B2; the root mean square error (RMSE) is 18.02 cm for Field B1 and 16.95 cm for Field B2; the regression  
 489 coefficient  $b$  is 0.94 and 1 for Fields B1 and B2, respectively. The general agreement between the measured and  
 490 simulated groundwater depth suggests that the two parameters are adequate, and the model can be used as a tool to  
 491 simulate the change of the groundwater depth.

492 Table 7-2

493 *Model statistics for validation of the Shallow Aquifer model in 2017- Mean relative error, MRE; root mean square*  
 494 *error, RMSE; Regression slope; Coefficient of determination, R2; Regression coefficient, b.*

		Validation (2017)						
		SWC						GWD
		0-10cm	10-30cm	30-50cm	50-70cm	70-90cm	0-90cm	
B1	MRE(%)	-0.76	19.48	-2.84	3.60	4.83	4.86	-4.11
	RMSE(cm <sup>3</sup> /cm <sup>3</sup> or cm)	0.02	0.07	0.03	0.03	0.03	0.03	18.02
	Regression Slope	1.03	0.57	1.38	1.49	0.70	0.76	0.80
	NSE	-0.70	0.58	0.53	0.29	0.78	0.66	0.84
	R <sup>2</sup>	0.39	0.65	0.87	0.88	0.88	0.69	0.84
	b	0.99	1.03	0.99	1.05	1.03	1.02	0.94
B2	MRE(%)	-3.67	-9.34	-6.34	-5.06	-1.75	-4.92	1.35
	RMSE(cm <sup>3</sup> /cm <sup>3</sup> or cm)	0.02	0.05	0.04	0.03	0.01	0.03	16.95
	Regression Slope	1.11	1.92	2.24	1.89	1.02	1.32	0.94
	NSE	-0.12	-3.07	-1.86	-0.81	0.63	0.02	0.85
	R <sup>2</sup>	0.62	0.68	0.90	0.90	0.83	0.74	0.86
	b	0.96	0.92	0.95	0.96	0.98	0.96	1.00

495 **4 Discussion**

496 In this manuscript, a novel surrogate model was developed for irrigation systems where the groundwater is  
 497 close to the surface. The model uses the soil moisture characteristic curve to derive the drainable porosity and to  
 498 predict the moisture contents in the soil. It is based on a less often used definition of field capacity (or equilibrium  
 499 moisture content as it is called in this manuscript) based on the observation that the flow becomes negligible when

500 the hydraulic gradient is zero. In other words, the system is in equilibrium when the sum of the matric potential and  
501 the gravity potential is constant. Thus, when we chose the groundwater level as the reference point for the gravity  
502 potential, the matric potential is equal to the height above the groundwater. This is different from other application  
503 of Darcy's law where the groundwater is below 3.3 m. In these cases, groundwater movement stops when the  
504 conductivity becomes negligible at -33 kPa or 3.3 m in head units. [The hydraulic conductivity value above -33 kPa  
505 \(3.3 m in head units\) does not limit the system reaching equilibrium for daily time steps. No need therefore exists to  
506 measure this parameter in great detail for surrogate models. The opposite is true for the soil moisture characteristic  
507 curve for determining the spatial distribution of moisture content with depth above the groundwater.](#)

508 In general, this [surrogate](#) model simulated the soil moisture content in each soil layer well, certainly when  
509 compared to other models that attempted the soil moisture contents in the Yellow River basin such as North China  
510 Plain (Kendy et al., 2003) and the Hetao Irrigation District by Gao et al. (2017b) [during the crop growth period](#). Our  
511 simulation results suggest that the reduction factor of the potential evaporation for soil saline  $K_c$  and root function  
512 parameters, together with the information of the soil [moisture](#) characteristic curves, can be used to adequately  
513 predict the soil moisture content. To predict the groundwater depth, two additional parameters are needed for the  
514 exponential function that defines the upward movement of groundwater.

515 The simulations, together with the observed data, [indicated](#) that information about the soil is very important to  
516 obtain the exact moisture content in the soil. However, generalized soil [moisture](#) characteristic curves for each soil  
517 type can be used in the simulation and will not result in great differences in water use by plants since percolation to  
518 deeper layers was negligible and thus the only loss of water was by [evapotranspiration](#) independent of the soil  
519 moisture content.

520 Finally, in the simulations we did not consider the influence of crop type and the influence of crop growth on  
521 soil moisture and groundwater depth. It would be of interest to investigate in future work whether the simulations  
522 would be improved by considering the dynamic crop characteristics during the growing season (Singh et al., 2018;  
523 Talebizadeh et al., 2018). A mature crop model, such as the EPIC model (Williams et al., 1989) that needs  
524 [relatively](#) few parameters, will certainly help to predict the crop yield but might not change the water use predictions.  
525 [Actually, the EPIC model already applied in Hetao irrigation district by many researchers to analyze the crop growth  
526 during the crop growth period \(Jia et al., 2012; Xu et al., 2015\).](#)

527 **5 Conclusion**

528 A novel surrogate vadose zone model for an irrigated area with a shallow aquifer was developed to simulate the  
529 fluctuation of groundwater depth and soil moisture during the crop growth stage in the shallow groundwater district.  
530 To validate and calibrate the surrogate model we carried out a two-year field experiment in the Hetao irrigation  
531 district in upper Mongolia with groundwater close to the surface. Using meteorological data and the soil moisture  
532 characteristic curve and upward capillary movement, the surrogate model predicted the soil water content with depth  
533 and groundwater height on daily time step with acceptable accuracy during validation and was an improvement two  
534 previous models applied in the Hatao district that could predict the overall water content in the root zone but not the  
535 distribution with depth.

536 The surrogate modeling results show that after an irrigation event as long as the upward flux from the  
537 groundwater to the root zone was greater than the plant evapotranspiration rate, the moisture contents in the vadose  
538 zone could be found directly from the soil moisture characteristic curve by equating the depth to the groundwater  
539 with the absolute value of the matric potential. When plant evapotranspiration rate exceeded the upward movement  
540 moisture contents would be indicated by groundwater depth and was predicted by a root zone function. Another  
541 finding was that the daily moisture contents were simulated without using the unsaturated hydraulic conductivity  
542 function in the surrogate model. For a daily time step equilibrium (defined as the hydraulic potential being constant)  
543 in moisture contents in the profile was attained so that precise unsaturated conductivity was not needed. Of course,  
544 for shorter time steps, predicting the transient fluxes and groundwater the conductivity function is needed. For  
545 management purposes a daily time step is acceptable.

546 Future improvement to this model will focus on coupling the EPIC model and apply it to simulate other crops  
547 and other location with shallow groundwater table. The surrogate model should also be compared with a “full”  
548 model, to test under what conditions the surrogate model will fall short.

549 **Data availability:** The observed data used in this study are not publicly accessible. These data have been collected  
550 by personnel the College of Water Resources and Civil Engineering, China Agricultural University, with fund from  
551 various cooperative sources. [Anyone who](#) would like to use these data, should contact Zhongyi Liu, Xingwang  
552 Wang and Zailin Huo to obtain permission.

553 **Competing interests:** The authors declare that they have no conflict of interest.

554 **Acknowledgements:**

555 This study was supported by National Key Research and Development Program of China (2017YFC0403301) and  
556 the National Natural Science Foundation of China (No. 51639009, 51679236). Peggy Stevens helped greatly with  
557 polishing the English. We thank Xingwang Wang who helped in collecting Field B2ata.

558 **References:**

559 [Abrahart, R.J and See, L.: Comparing neural network and autoregressive moving average techniques for the](#)  
560 [provision of continuous river flow forecasts in two contrasting catchments. \*Hydro. Processes\*. 14: 2157-2172.](#)  
561 [http://doi.org/10.1002/1099-1085\(20000815/30\)14:11/12<2157::AID-HYP57>3.0.CO;2-S](http://doi.org/10.1002/1099-1085(20000815/30)14:11/12<2157::AID-HYP57>3.0.CO;2-S). 2000.

562 [Alcamo, J., Florke, M., and Marker, M.: Future long-term changes in global water resources driven by socio-](#)  
563 [economic and climatic changes. \*Hydrolog Sci J.\*, 52:247-275, https://doi.org/10.1623/hysj.52.2.247](#). 2007.

564 [Allen, R.G., Pereira, L.S., Raes, D., and Smith, M.: Crop evapotranspiration. Guidelines for computing crop water](#)  
565 [requirements-FAO Irrigation and Drainage Paper 56, FAO, Rome](#). 1998

566 [Asher, M.J., Croke, B.F.W., Jakeman, A.J. and Peeters, L.J.M.: A review of surrogate models and their application](#)  
567 [to groundwater modeling. \*Water Resour Res\* 51:5957-5973. http://doi.wiley.com/10.1002/2015WR016967](#).  
568 2015.

569 [Bahmani, O., and Bayram, M.: Investigating the hydraulic conductivity and soil characteristics under compaction](#)  
570 [and soil texture and performances as landfill liner. \*Arab J Geosci.\*, 11\(16\): 453. https://](#)  
571 [doi.org/10.1007/s12517-018-3817-7](https://doi.org/10.1007/s12517-018-3817-7). 2018.\

572 [Batalha, M.S., Barbosa, M.C., Faybishenko, B., van Genuchten, M.T.: Effect of temporal averaging of](#)  
573 [meteorological data on predictions of groundwater recharge. \*J Hydrol Hydromech\*, 66\(2\):143-152.](#)  
574 <https://doi.org/10.1515/johh-2017-0051>. 2018.

575 [Bauters, T.W.J., Steenhuis, T.S., Dicarolo, D.A., Nieber, J.L., Dekker, L.W., Ritsema, C.J., Parlange, J.Y., and](#)  
576 [Haverkamp, R.: Physics of water repellent soils. \*J. Hydrol.\*, SI: 233-243](#). 2000.

577 [Beven, K.J., and Kirkby, M.J.: A physically based, variable contributing area model of basin hydrology. \*Hydrolog\*  
578 \[Sci J.\]\(#\), 24:43-69. <https://doi.org/10.1080/02626667909491834>. 1979.](#)

579 [Brooks, E.S., Boll, J., McDaniel, P.A.: Distributed and integrated response of a geographic information system-](#)  
580 [based hydrologic model in the eastern Palouse region, Idaho. \*Hydro. Processes\*. 21:110-122. http://doi.org/10.1](#)  
581 [002/hyp.6230](http://doi.org/10.1002/hyp.6230). 2007.

582 [Brooks, R.H., and Corey, A.T.: Hydraulic properties of porous media, Hydrology Paper 3. Colorado State](#)  
583 [University. Fort Collins, Colorado, 37pp](#), 1964.

584 [Bowden, G.J., Maier, H.R. and Dandy, G.C.. Optimal division of data for neural network models in water resources](#)  
585 [applications. \*Water Resour Res\* 38:2-1-2-11. https://doi.org/10.1029/2001WR000226](#).2002

586 Brown, A and Matlock, M.D.: A review of water scarcity indices and methodologies. White paper 106. University  
587 of Arkansas. The Sustainability Consortium. 26pp. 2011.

588 Chen, C., Wang, E., and Yu, Q.: Modelling the effects of climate variability and water management on crop water  
589 productivity and water balance in the North China Plain. *Agr. Water Manage.*, 97:1175-1184. <https://doi.org/10.1016/j.agwat.2008.11.012>. 2010.

591 Cui, T., Peeters, L., Pagendam, D., Pickett, T., Jin, H., Crosbie, R., Raiber, M., Rassam, D., and Gilfedder, M.:  
592 Emulator-enabled approximate Bayesian computation (ABC) and uncertainty analysis for computationally  
593 expensive groundwater models. *J Hydrol* 564:191-207. <https://doi.org/10.1016/j.jh.ydrol.2018.07.005>

594 Dam, J.C. Van., Huygen, J, Wesseling, JG, Feddes, RA., Kabat, P.,Walsum, PEV. Van.,Groenendijk, P., Diepen.:  
595 Theory of SWAP version 2.0. Simulation of water flow, solute transport and plant growth in the soil-water-  
596 atmosphere-plant environment. Report 71, Department Water Resources, Wageningen Agricultural University.  
597 Technical document 45, DLO Winand Staring Centre, Wageningen,152pp, 1997.

598 Dawson, C.W., Abrahart, R.J., Shamseldin, A.Y., Wilby, R.L.: Flood estimation at ungauged sites using artificial  
599 neural networks. *J Hydrol.*319: 391-409. <http://doi.org/10.1016/j.jhydrol.2005.07.032>. 2006.

600 Falkenmark, M.: The Massive Water Scarcity Now Threatening Africa: Why Isn't It Being Addressed? *Ambio.*18:  
601 112-118.1989

602 Flint, A.L., Flint, L.E., Kwicklis, E.M., Fabryka-Martin, J.T., and Bodvarsson, G.S.: Estimating recharge at Yucca  
603 Mountain, Nevada, USA: comparison of methods. *Hydrogeol. J.*, 10:180-204. <https://doi.org/10.1007/s10040-001-0169-1>. 2002.

605 Gao, X., Huo, Z., Qu, Z., Xu, X., Huang, G., and Steenhuis, T.S.: Modeling contribution of shallow groundwater to  
606 evapotranspiration and yield of maize in an arid area. *Sci. Rep-UK* 7. <https://doi.org/10.1038/srep43122>. 2017a.

607 Gao, X., Huo, Z., Bai, Y., Feng, S., Huang, G., Shi, H., and Qu, Z.: Soil salt and groundwater change in flood  
608 irrigation field and uncultivated land: a case study based on 4-year field observations. *Environ. Earth Sci.*,  
609 73:2127-2139. <https://doi.org/10.1007/s12665-014-3563-4>. 2015.

610 Gao, X., Bai, Y., Huo, Z., Xu, X., Huang, G., Xia, Y., and Steenhuis, T.S.: Deficit irrigation enhances contribution  
611 of shallow groundwater to crop water consumption in arid area. *Agr. Water Manage.*, 185:116-125. <https://doi.org/10.1016/j.agwat.2017.02.012>. 2017b.

613 Gardner, W.: Some steady-state solutions of the unsaturated moisture flow equation with application to evaporation  
614 from a water table. *Soil Sci.*, 85:228-232. 1958.

615 Gardner, W., Hillel, D., and Benyamini, Y.: Post-Irrigation Movement Soil Water 1. Redistribution. *Water Resour.*  
616 *Res.*, 6:851-860. <https://doi.org/10.1029/WR006i003p00851>. 1970a.

617 Gardner, W., Hillel, D., and Benyamini, Y.: Post-Irrigation Movement of Soil Water 2. Simultaneous Redistribution  
618 and Evaporation. *Water Resour. Res.*, 6:1148-1153. <https://doi.org/10.1029/WR006i004p01148>. 1970b.

619 Gleeson, T., Befus, K.M., Jasechko, S., Luijendijk, E., and Cardenas, M.B.: The global volume and distribution of  
620 modern groundwater. *Nat. Geosci.*, 9:161-167. <https://doi.org/10.1038/NGEO2590>. 2016.

621 Guo, S., Ruan, B., Chen, H., Guan, X., Wang, S., Xu, N. and Li, Y.: Characterizing the spatiotemporal evolution of  
622 soil salinization in Hetao Irrigation District (China) using a remote sensing approach. *Int J Remote Sens*  
623 39:6805-6825. <https://doi.org/10.1080/01431161.2018.1466076>. 2018.

624 Guo, Y., and Shen, Y.: Agricultural water supply/demand changes under projected future climate change in the arid  
625 region of northwestern China. *J. Hydrol*, 540:257-273. <https://doi.org/10.1016/j.jhydrol.2016.06.033>. 2016.

626 Gupta, S., and Larson, W.: Estimating Soil Water Retention Characteristics From Particle Size Distribution, Organic  
627 Matter Percent, and Bulk Density. *Water Resour. Res.*, 15:1633-1635. [https://](https://doi.org/10.1029/WR015i006p01633)  
628 [doi.org/10.1029/WR015i006p01633](https://doi.org/10.1029/WR015i006p01633). 1979.

629 Haverkamp, R., and Parlange, J.: Predicting the Water-Retention Curve from Particle-Size Distribution: 1. Sandy  
630 Soils Without Organic Matter. *Soil Sci.*, 142:325-339. [https:// doi.org/10.1097/00010694-198612000-00001](https://doi.org/10.1097/00010694-198612000-00001).  
631 1986.

632 Hinrichsen, D., Henrylito D.T.: *The Coming Freshwater Crisis is Already Here. Finding the Source: The Linkages*  
633 *Between Population and Water. Environmental Change and Security Program, Washington, DC, 26pp, 2002.*

634 Hoang, L., Schneiderman, E.M., Moore, K.E.B., Mukundan, R., Owens, E.M., and Steenhuis, T.S.: Predicting  
635 saturation-excess runoff distribution with a lumped hillslope model: SWAT-HS. *Hydrol. Process.*, 31:2226-  
636 2243. [https:// doi.org/ 10.1002/hyp.11179](https://doi.org/10.1002/hyp.11179). 2017.

637 Hodnett, M., and Bell, J. Soil moisture investigations of groundwater recharge through black cotton soils in Madhya  
638 Pradesh, India. *Hydrolog Sci J* 31:361-381. [https:// doi.org/10.1080/02626668609491054](https://doi.org/10.1080/02626668609491054). 1986.

639 Huang, Q., Xu, X., Lu, L., Ren, D., Ke, J., Xiong, Y., Huo, Z. and Huang, G.: Soil salinity distribution based on  
640 remote sensing and its effect on crop growth in Hetao Irrigation District. *Transactions of the Chinese Society of*  
641 *Agricultural Engineering* 34:102-109. 2018.

642 Jakeman, A.J., Letcher, R.A., Norton, J.P.: Ten iterative steps in development and evaluation of environmental  
643 models. *Environ Modell Softw.* 21:602-614. [https:// doi.org/ 10.1016/j.envsoft.2006.01.004](https://doi.org/10.1016/j.envsoft.2006.01.004). 2006.

644 Jasechko, S., and Taylor, R.G.: Intensive rainfall recharges tropical groundwaters. *Environ. Res. Lett.*, 10:124015.  
645 [https:// doi.org/10.1088/1748-9326/10/12/124015](https://doi.org/10.1088/1748-9326/10/12/124015). 2015.

646 Jia, H., Wang, J., Cao, C., Pan, D., Shi, P.: Maize drought disaster risk assessment of China based on EPIC model.  
647 *International Journal of Digital Earth.* 5:488-515. [https:// doi.org/10.1080/17538947.2011.590535](https://doi.org/10.1080/17538947.2011.590535). 2012.

648 Kahlowan, M., Ashraf, M., and Zia-Ul-Haq.: Effect of shallow groundwater table on crop water requirements and  
649 crop yields. *Agr. Water Manage.*, 76:24-35. [https:// doi.org/10.1016/j.agwat.2005.01.005](https://doi.org/10.1016/j.agwat.2005.01.005). 2005.

650 Katerji, N., van Hoorn, J.W., Hamdy, A., and Mastrorilli, M.: Salinity effect on crop development and yield,  
651 analysis of salt tolerance according to several classification methods. *Agr. Water Manage.*, 62:37-66. [https://](https://doi.org/10.1016/S0378-3774(03)00005-2)  
652 [doi.org/10.1016/S0378-3774\(03\)00005-2](https://doi.org/10.1016/S0378-3774(03)00005-2). 2003.

653 Kendy, E., Gérard-Marchant, P., Walter, M. T., Zhang, Y., Liu, C., and Steenhuis, T.S.: A soil-water-balance  
654 approach to quantify groundwater recharge from irrigated cropland in the North China Plain. *Hydrol. Process.*,  
655 17:2011-2031. [https:// doi.org/10.1002/hyp.1240](https://doi.org/10.1002/hyp.1240). 2003.

656 Kirchner, J. W., Getting the right answers for the right reasons: Linking measurements, analyses, and models to  
657 advance the science of hydrology, *Water Resour. Res.*, 42, W03S04, <https://doi.org/10.1029/2005WR004362>.  
658 2006.

659 Krause, P., Boyle, D.P. and B äse, F.: Comparison of different efficiency criteria for hydrological model assessment.  
660 *Advances in Geosciences* 5:89-97. [https:// doi.org/ 10.5194/adgeo-5-89-2005](https://doi.org/10.5194/adgeo-5-89-2005). 2005.

661 Langevin, C.D., Hughes, J.D., Banta, E.R., Niswonger, R.G., Panday, Sorab, and Provost, A.M. Documentation for  
662 the MODFLOW 6 Groundwater Flow Model: U.S. Geological Survey Techniques and Methods, book 6, chap.  
663 A55, 197 p., <https://doi.org/10.3133/tm6A55>. 2017.

664 Li, C., Yang, Z., and Wang, X.: Trends of Annual Natural Runoff in the Yellow River Basin. *Water Int.*, 29:447-454.  
665 [https:// doi.org/10.1080/02508060408691807](https://doi.org/10.1080/02508060408691807). 2004.



666 Li, X., Zhao, Y., Xiao, W., Yang, M., Shen, Y., Min, L.: Soil moisture dynamics and implications for irrigation of  
667 farmland with a deep groundwater table. *Agr. Water Manage.*,192:138-148. [https:// doi.org/  
668 10.1016/j.agwat.2017.07.003](https://doi.org/10.1016/j.agwat.2017.07.003). 2017.

669 Liu, Z., Chen, H., Huo, Z., Wang, F., and Shock, C.C.: Analysis of the contribution of groundwater to  
670 evapotranspiration in an arid irrigation district with shallow water table. *Agr. Water Manage.*, 171:131-141.  
671 [https:// doi.org/10.1016/j.agwat.2016.04.002](https://doi.org/10.1016/j.agwat.2016.04.002). 2016.

672 Luan, X., Wu, P., Sun, S., Wang, Y., and Gao, X.: Quantitative study of the crop production water footprint using  
673 the SWAT model. *Ecol. Indic.*, 89:1-10. [https:// doi.org/10.1016/j.ecolind.2018.01.046](https://doi.org/10.1016/j.ecolind.2018.01.046). 2018.

674 Luo, Y., and Sophocleous, M.: Seasonal groundwater contribution to crop-water use assessed with lysimeter  
675 observations and model simulations. *J. Hydrol.*, 389:325-335. [https:// doi.org/10.1016/j.jhydrol.2010.06.011](https://doi.org/10.1016/j.jhydrol.2010.06.011).  
676 2010.

677 Ma, Y., Feng, S., and Song, X.: A root zone model for estimating soil water balance and crop yield response to  
678 deficit irrigation in the North China Plain. *Agr. Water Manage.*, 127:13-24. [https://  
679 doi.org/10.1016/j.agwat.2013.05.011](https://doi.org/10.1016/j.agwat.2013.05.011). 2013.

680 Matott, L.S., and Rabideau, A.J.: Calibration of complex subsurface reaction models using a surrogate-model  
681 approach. *Adv Water Resour* 31:1697-1707. [https:// doi.org/10.1016/j.advwatres.2008.08.006](https://doi.org/10.1016/j.advwatres.2008.08.006).  
682 2008.

683 Mccuen, R., Rawls, W., and Brakensiek, D.: Statistical Analysis of the Brooks-Corey and the Green-Ampt  
684 Parameters. *Water Resour. Res.*, 17:1005-1013. [https:// doi.org/10.1029/WR017i004p01005](https://doi.org/10.1029/WR017i004p01005). 1981.

685 Mcdonald, M., and Harbaugh, A.: The history of MODFLOW. *Groundwater* 41:280-283. [https://  
686 doi.org/10.1111/j.1745-6584.2003.tb02591.x](https://doi.org/10.1111/j.1745-6584.2003.tb02591.x). 2003.

687 Moges, M., Schmitter, P., Tilahun, S., Langan, S., Dagnew, D., Akale, A. and Steenhuis, T.S.: Suitability of  
688 Watershed Models to Predict Distributed Hydrologic Response in the Awramba Watershed in Lake Tana Basin.  
689 *Land Degrad Dev* 10:1386-1397. [https:// doi.org/10.1002/ldr.2608](https://doi.org/10.1002/ldr.2608). 2017.

690 Moiwo, J.P., Lu, W., Zhao, Y., Yang, Y., and Yang, Y.: Impact of land use on distributed hydrological processes in  
691 the semi-arid wetland ecosystem of Western Jilin. *Hydrol. Process.*, 24:492-503. [https://  
692 doi.org/10.1002/hyp.7503](https://doi.org/10.1002/hyp.7503). 2010.

693 Moriasi, D.N., Arnold, J.G., Van Liew, M.W., Bingner, R.L., Harmel, R.D., Model evaluation guidelines for  
694 systematic quantification of accuracy in watershed simulations. *T. ASABE.* 50:885-900. 2007.

695 Nash, J.E., and Sutcliffe, J.V.: River flow forecasting through conceptual models part I – a discussion of principles.  
696 *J Hydrol* 10:282-290. 1970.

697 Oki, T., and Kanae, S.: Global Hydrological Cycles and World Water Resources. *Science*, 313:1068-1072. [https://  
698 doi.org/10.1126/science.1128845](https://doi.org/10.1126/science.1128845). 2006.

699 Razavi, S., Tolson, B.A. and Burn, D.H. Review of surrogate modeling in water resources. *Water Resour Res* 48.  
700 [https:// doi.org/10.1029/2011WR011527](https://doi.org/10.1029/2011WR011527). 2012a.

701 Razavi, S., Tolson, B.A. and Burn, D.H.: Numerical assessment of metamodelling strategies in computationally  
702 intensive optimization. *Environ Modell Softw.* 34:67-86. [https:// doi.org/10.1016/ j.envsoft.2011.09.010](https://doi.org/10.1016/j.envsoft.2011.09.010). 2012b.

703 Ren, D., Xu, X., Hao, Y., and Huang, G.: Modeling and assessing field irrigation water use in a canal system of  
704 Hetao, upper Yellow River basin: Application to maize, sunflower and watermelon. *J. Hydrol.*, 532:122-139.  
705 [https:// doi.org/10.1016/j.jhydrol.2015.11.040](https://doi.org/10.1016/j.jhydrol.2015.11.040). 2016.

706 Ren, D., Xu, X., Engel, B., and Huang, G.: Growth responses of crops and natural vegetation to irrigation and water  
707 table changes in an agro-ecosystem of Hetao, upper Yellow River basin: Scenario analysis on maize, sunflower,  
708 watermelon and tamarisk. *Agr. Water Manage.*, 199:93-104. [https:// doi.org/10.1016/j.agwat.2017.12.021](https://doi.org/10.1016/j.agwat.2017.12.021). 2018.

709 [Renewable internal freshwater resources per capita \(cubic meters\)](https://data.worldbank.org/indicator/ER.H2O.IN). <https://data.worldbank.org/indicator/ER.H2O.IN>  
710 [TR.PC.2019](https://data.worldbank.org/indicator/ER.H2O.IN).

711 Ritter, A., and Muñoz-Carpena, R.: Performance evaluation of hydrological models: Statistical significance for  
712 reducing subjectivity in goodness-of-fit assessments. *J Hydrol* 480:33-45. 2013.[htt p:// doi.org/](https://doi.org/10.1016/j.jhydrol.2012.12.004)  
713 [10.1016/j.jhydrol.2012.12.004](https://doi.org/10.1016/j.jhydrol.2012.12.004). 2013.

714 Rodriguez-Iturbe, I.: Ecohydrology: A hydrologic perspective of climate-soil-vegetation dynamics. *Water Resour.*  
715 *Res.*, 36:3-9. [https:// doi.org/10.1029/1999WR900210](https://doi.org/10.1029/1999WR900210). 2000.

716 Rosa, R.D., Paredes, P., Rodrigues, G.C., Alves, I, Fernando, R.M., Pereira, L.S., Allen, R.G.: Implementing the  
717 dual crop coefficient approach in interactive software. 1. Background and computational strategy. *Agr. Water*  
718 *Manage.*,103: 8-24. [https:// doi.org/10.1016/j.agwat.2011.10.013](https://doi.org/10.1016/j.agwat.2011.10.013). 2012.

719 Saleh, A., Steenhuis, T.S., and Walter, M.: Groundwater table simulation under different rice irrigation practices. *J*  
720 *Irrig Drain Eng* 115:530-544. [https:// doi.org/10.1061/\(ASCE\)0733-9437\(1989\)115:4\(530\)](https://doi.org/10.1061/(ASCE)0733-9437(1989)115:4(530)). 1989.

721 Šimůnek, J., Šejna, M. and van Genuchten, M.T.: The HYDRUS-1D software package for simulating the one-  
722 dimensional movement of water, heat, and multiple solutes in variably-saturated media. Version 2.0. IGWMC-  
723 TPS-70. *Int. Groundwater Modeling Ctr., Colorado School of Mines, Golden*. 1998.

724 Singh, L.K., Jha, M.K., and Pandey, M.: Framework for Standardizing Less Data-Intensive Methods of Reference  
725 Evapotranspiration Estimation. *Water Resour. Manag.*, 32:4159-4175. [https:// doi.org/10.1007/s11269-018-](https://doi.org/10.1007/s11269-018-2022-5)  
726 [2022-5](https://doi.org/10.1007/s11269-018-2022-5). 2018.

727 Sun, S., Wu, P., Wang, Y., Zhao, X., Liu, J., and Zhang, X.: The impacts of interannual climate variability and  
728 agricultural inputs on water footprint of crop production in an irrigation district of China. *Sci. Total Environ.*,  
729 444:498-507. [https:// doi.org/10.1016/j.scitotenv.2012.12.016](https://doi.org/10.1016/j.scitotenv.2012.12.016). 2013.

730 Talebizadeh, M., Moriasi, D., Gowda, P., Steiner, J.L., Tadesse, H.K., Nelson, A.M., and Starks, P.: Simultaneous  
731 calibration of evapotranspiration and crop yield in agronomic system modeling using the APEX model. *Agr.*  
732 *Water Manage.*, 208:299-306. [https:// doi.org/10.1016/j.agwat.2018.06.043](https://doi.org/10.1016/j.agwat.2018.06.043). 2018.

733 Todini, E.: [Hydrological catchment modelling: past, present and future](https://doi.org/10.5194/hess-11-468-2007). *Hydrol Earth Syst Sc* 11:468-482. [https://](https://doi.org/10.5194/hess-11-468-2007)  
734 [doi.org/10.5194/hess-11-468-2007](https://doi.org/10.5194/hess-11-468-2007). 2007.

735 van Genuchten, M.T.: A Closed-form Equation for Predicting the Hydraulic Conductivity of Unsaturated Soils. *Soil*  
736 *Sci. Soc. Am. J.*, 44:892-898. [https:// doi.org/10.2136 /sssaj1980.03615995004400050002x](https://doi.org/10.2136/sssaj1980.03615995004400050002x). 1980.

737 Venkatesh, B., Lakshman, N., Purandara, B.K., and Reddy, V.B.: Analysis of observed soil moisture patterns under  
738 different land covers in Western Ghats, India. *J. Hydrol*, 397:281-294. [https://](https://doi.org/10.1016/j.jhydrol.2010.12.006)  
739 [doi.org/10.1016/j.jhydrol.2010.12.006](https://doi.org/10.1016/j.jhydrol.2010.12.006). 2011.

740 Wang, E., and Smith, C.J.: Modelling the growth and water uptake function of plant root systems: a review. *Aust. J.*  
741 *Agr. Res.*, 55:501. [https:// doi.org/10.1071/AR03201](https://doi.org/10.1071/AR03201). 2004.

742 Wang, H., Tetzlaff, D., and Soulsby, C.: Modelling the effects of land cover and climate change on soil water  
743 partitioning in a boreal headwater catchment. *J. Hydrol*, 558:520-531. [https://](https://doi.org/10.1016/j.jhydrol.2018.02.002)  
744 [doi.org/10.1016/j.jhydrol.2018.02.002](https://doi.org/10.1016/j.jhydrol.2018.02.002). 2018.

745 Wang, H., Zhang, L., Dawes, W.R., and Liu, C.: Improving water use efficiency of irrigated crops in the North  
746 China Plain - measurements and modelling. *Agr. Water Manage.*, 48:151-167. [https:// doi.org/10.1016/S0378-](https://doi.org/10.1016/S0378-3774(00)00118-9)  
747 [3774\(00\)00118-9](https://doi.org/10.1016/S0378-3774(00)00118-9). 2001.

748 Wang, X., Huo, Z., Guan, H., Guo, P., and Qu, Z.: Drip irrigation enhances shallow groundwater contribution to  
749 crop water consumption in an arid area. *Hydrol. Process.*, 32:747-758. [https:// doi.org/10.1002/hyp.11451](https://doi.org/10.1002/hyp.11451). 2018.

750 Williams, J., Prebble, R., Williams, W., and Hignett, C.: The influence of texture, structure and clay mineralogy on  
751 the soil moisture characteristic. *Aust. J. Soil Res.*, 21:15-32. [https:// doi.org/10.1071/SR9830015](https://doi.org/10.1071/SR9830015). 1983.

752 Williams, J., Jones, C., Kiniry, J., and Spanel, D.: The EPIC Crop Growth Model. *T. ASAE*, 32:479-511. 1989.

753 Xu, X., Huang, G., Qu, Z., and Pereira, L.S.: Assessing the groundwater dynamics and impacts of water saving in  
754 the Hetao Irrigation District, Yellow River basin. *Agr. Water Manage.*, 98:301-313. [https://  
755 doi.org/10.1016/j.agwat.2010.08.025](https://doi.org/10.1016/j.agwat.2010.08.025). 2010.

756 Xu, X., Sun, C., Qu, Z., Huang, Q., Ramos, T.B., and Huang, G.: Groundwater Recharge and Capillary Rise in  
757 Irrigated Areas of the Upper Yellow River Basin Assessed by an Agro-Hydrological Model. *Irrig. Drain.*,  
758 64:587-599. [https:// doi.org/10.1002/ird.1928](https://doi.org/10.1002/ird.1928). 2015.

759 Xue, J., Huo, Z., Wang, F., Kang, S., and Huang, G.: Untangling the effects of shallow groundwater and deficit  
760 irrigation on irrigation water productivity in arid region: New conceptual model. *Sci. Total Environ.*, 619-  
761 620:1170-1182. [https:// doi.org/10.1016/j.scitotenv.2017.11.145](https://doi.org/10.1016/j.scitotenv.2017.11.145). 2018.

762 Yang, F., Zhang, G., Yin, X., Liu, Z., and Huang, Z.: Study on capillary rise from shallow groundwater and critical  
763 water table depth of a saline-sodic soil in western Songnen plain of China. *Environ. Earth Sci.*, 64:2119-2126.  
764 [https:// doi.org/10.1007/s12665-011-1038-4](https://doi.org/10.1007/s12665-011-1038-4). 2011.

765 Yang, X., Chen, Y., Pacenka, S., Gao, W., Ma, L., Wang, G., Yan, P., Sui, P., and Steenhuis, T.S.: Effect of  
766 diversified crop rotations on groundwater levels and crop water productivity in the North China Plain. *J.*  
767 *Hydrol.*, 522:428-438. [https:// doi.org/ 10.1016/j.jhydrol.2015.01.010](https://doi.org/10.1016/j.jhydrol.2015.01.010). 2015a.

768 Yang, X., Chen, Y., Pacenka, S., Gao, W., Zhang, M., Sui, P., and Steenhuis, T.S.: Recharge and Groundwater Use  
769 in the North China Plain for Six Irrigated Crops for an Eleven Year Period. *Plos One* 10:e0115269. [https://  
770 doi.org/10.1371/journal.pone.0115269](https://doi.org/10.1371/journal.pone.0115269). 2015b.

771 Yang, X., Chen, Y., Steenhuis, T.S., Pacenka, S., Gao, W., Ma, L., Zhang, M., and Sui, P.: Mitigating Groundwater  
772 Depletion in North China Plain with Cropping System that Alternate Deep and Shallow Rooted Crops. *Front.*  
773 *Plant Sci.*, 8. [https:// doi.org/ 10.3389/fpls.2017.00980](https://doi.org/10.3389/fpls.2017.00980). 2017.

774 Yeh, P.J., and Famiglietti, J.S.: Regional Groundwater Evapotranspiration in Illinois. *J. Hydrometeorol.*, 10:464-478.  
775 [https:// doi.org/ 10.1175/2008JHM1018.1](https://doi.org/10.1175/2008JHM1018.1). 2009.

776 Young, P.C., and M. Ratto. *Statistical Emulation of Large Linear Dynamic Models. Technometrics* 53:29-43. [http://  
777 doi.org/ 10.1198/TECH.2010.07151](http://doi.org/10.1198/TECH.2010.07151). 2011.

778 Zammouri, M.: Case Study of Water Table Evaporation at Ichkeul Marshes (Tunisia). *J. Irrig. Drain. Eng.*, 127:265-  
779 271. [https:// doi.org/10.1061/\(ASCE\)0733-9437\(2001\)127:  
780 5\(265\)](https://doi.org/10.1061/(ASCE)0733-9437(2001)127:5(265)) . 2001.